Electronic Supplementary Information

# State- and Water Repellency-Controllable Molecular Glass of Pillar[5]arene with Fluoroalkyl Groups by Guest Vapors

Katsuto Onishi, Shunsuke Ohtani, Kenichi Kato, Shixin Fa, Yoko Sakata, Shigehisa Akine, Moe Ogasawara, Hitoshi Asakawa, Shusaku Nagano, Yoshinori Takashima, Motohiro Mizuno and Tomoki Ogoshi*

## Table of Contents

## 1. General

### 1.1 Solution Nuclear Magnetic Resonance (NMR)

Solution $^{1}H$ and $^{19}F$ NMR spectra were recorded at 400, and 376 MHz with a JNM-ECS400 spectrometer (JEOL RESONANCE Inc., Tokyo, Japan) and solution $^{13}C$ NMR spectra were recorded at 151 MHz a JNM-ECZ600R spectrometer with cold probe (ECZ600) (JEOL RESONANCE Inc., Tokyo, Japan). $^{1}H$ and $^{13}C$ chemical shifts were expressed as values relative to tetramethylsilane (TMS). $^{19}F$ chemical shifts were expressed by using the −78.8 ppm line of sodium trifluoromethanesulfonate as an external reference.

### 1.2 Powder X-Ray Diffraction (PXRD)

PXRD measurement was performed PXRD measurement was performed by a MiniFlexII (Rigaku Co., Tokyo, Japan).

### 1.3 Differential Scanning Calorimetry (DSC)

Results of DSC was obtained by a DSC7020 (Hitachi High-Tech Science Co., Tokyo, Japan) under a flow of dry nitrogen.

### 1.4 Transmittance Measurements

Transmittances of the compounds at 500 nm were recorded with a JASCO V-750 spectrophotometer. The compounds were coated on a Quartz plate.

### 1.5 Density Functional Theory (DFT) Calculations

The Gaussian 16 program package[S1] was used for computation. We optimized the structures of **F5** and **C1** in the ground state. The DFT was applied for the optimization of the structures in the ground states at B3LYP/6-31G(d,p) level.

### 1.6 Thermogravimetry-differential Thermal Analysis (TG-DTA) and Thermogravimetric Analysis (TGA)

Results of TG-DTA and TGA were obtained by a STA7200 (Hitachi High-Tech Science Co., Tokyo, Japan) under a flow of dry nitrogen.

### 1.7 Contact Angle Measurements

Contact angle values of the compounds were obtained by a Phoenix-Alpha P200A (Meiwafosis Co., Ltd., Tokyo, Japan). The compounds were coated on a glass substrate.

### 1.8 Atomic Force Microscopy (AFM) Analyses

A laboratory-built AFM with a commercially-available controller (ARC2, Asylum Research, Oxford Instruments) was used for the AFM analyses. Before all AFM experiments, a tip side of AFM cantilevers (160AC-NG, MikroMasch) was coated with Si (thickness: 30 nm) by a magnetron sputter coater (QT150, Quorum Technologies).[S2] After fixing a sample glass substrate with glue on a holder, the surface structures were analyzed in the air with the AFM system operated in amplitude modulation (AM) mode, known as tapping mode. The cantilever vibration was excited at its resonance frequency (nominal value was 300 kHz in air). The typical value of free vibration amplitude was 30 nm. The setpoint amplitude for tip-sample distance control was set around 70% of the free vibration amplitude.

### 1.9 Solid Nuclear Magnetic Resonance (NMR)

Solid-state $^{13}C$ NMR spectra were measured using a JEOL ECA-300 spectrometer operating at 74.175 MHz. High-resolution solid-state NMR spectrum was obtained using magic-angle spinning (MAS) and high-power 1 H dipole decoupling (DD). Cross-polarization (CP) was used for signal enhancement. The sample was packed into a 4 mm diameter zirconia rotor. The total suppression of sidebands (TOSS) sequence was used to suppress spinning sidebands. The MAS rate was set to 5 kHz. $^{13}C$ chemical shifts were expressed as values relative to tetramethylsilane (TMS) using the 29.50 ppm line of adamantane as an external reference.

### 1.10 Single-crystal X-ray Structural Analyses

Intensity data were collected on a Bruker D8 Venture diffractometer (with Cu Kα radiation, $\lambda$ = 1.54178 Å). The data were corrected for Lorentz and polarization factors and for absorption by semiempirical methods based on symmetry-equivalent and repeated reflections. The structure was solved by direct methods (SHELXT, SHELXS97, or SIR97) and refined by full-matrix least squares on $F^2$ using SHELXL 2014.[S3] Crystallographic data has been deposited with the Cambridge Crystallographic Data Centre under reference numbers CCDC 2121263–2121267 and 2144343. These data can be obtained free of charge via www.ccdc.cam.ac.uk/data_request/cif (or from the Cambridge Crystallographic Data Centre, 12 Union Road, Cambridge CB2 1EZ, UK).

## 2. Synthesis

**F5**. To a flask containing pillar[5]arene with 10 hydroxyl groups (0.650 g, 1.07 mmol) was added dry DMF (15 mL), dry THF (15 mL) and NaH (0.830 g, 33.4 mmol). The resulting mixture was stirred at 60 °C for 72 h under a nitrogen atmosphere where after 4,4,5,5,5-pentafluoropentyl 4-methylbenzenesulfonate[S4] (7.15 g, 21.5 mmol) was added. The reaction mixture was quenched with methanol, washed with brine, and dried over anhydrous $Na_2SO_4$. After filtration, the solvent was evaporated under reduced pressure. Column chromatography (silica gel; *n*-hexane:DCM = 4:1) afforded a white solid (308 mg, 0.139 mmol, yield 13%).

**Scheme S1** Synthesis of **F5**.

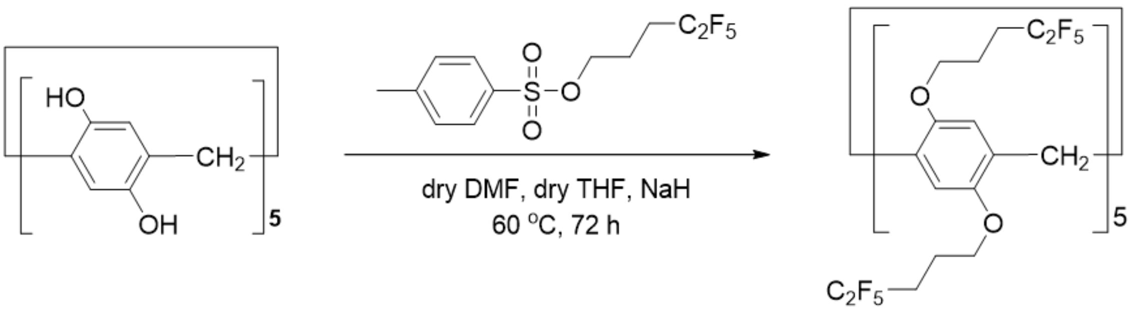


$^1$H NMR (**Fig. S1**, 400 MHz, $CDCl_3$, 25 °C) δ 6.76 (s, 10H), 3.75–4.03 (m, 20H), 3.73 (s, 10H), 2.25–2.34 (m, 20H), 2.08–2.11 (m, 20H); $^{13}$C NMR (**Fig. S2**, 151 MHz, $CDCl_3$, 25 °C) δ 149.8, 128.6, 115.4, 114.0–122.2, 67.3, 29.4, 27.9, 21.2; $^{19}$F NMR (**Fig. S3**, 376 MHz, $CDCl_3$, 25 °C) δ −86.0, −118.7; MS (APCI) calcd. for $C_{85}H_{81}O_{10}F_{50}$ $[M + H]^+$: 2211.4962, found 2211.5026.

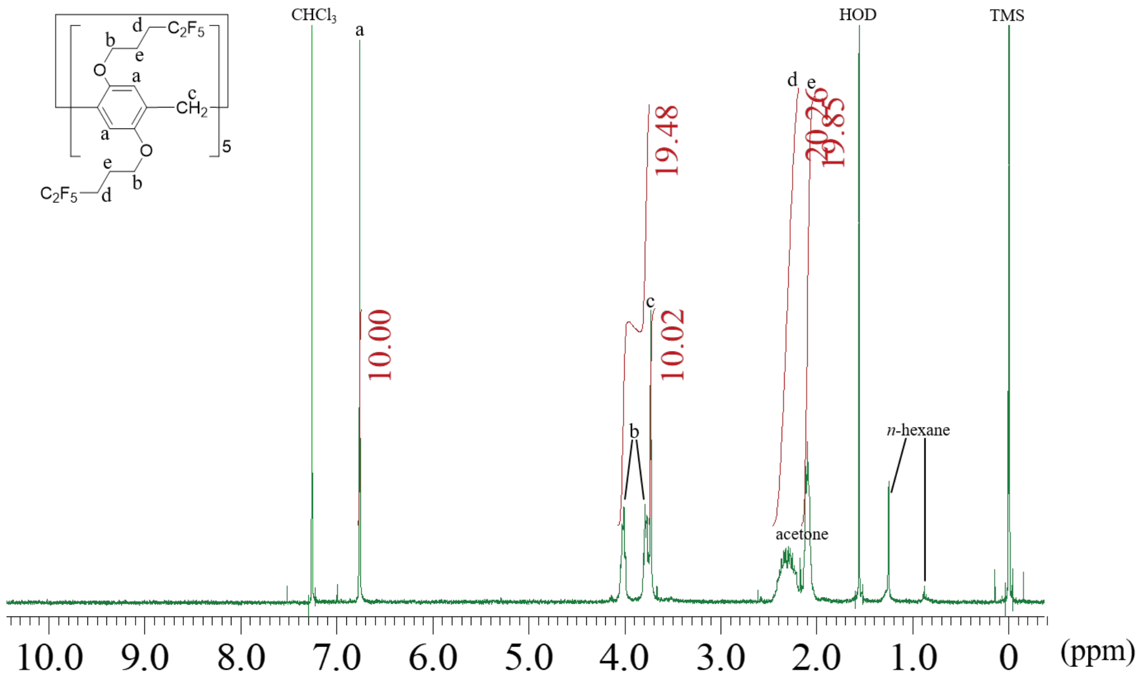


**Fig. S1** $^1$H NMR spectrum of **F5** ($CDCl_3$, 25 °C).

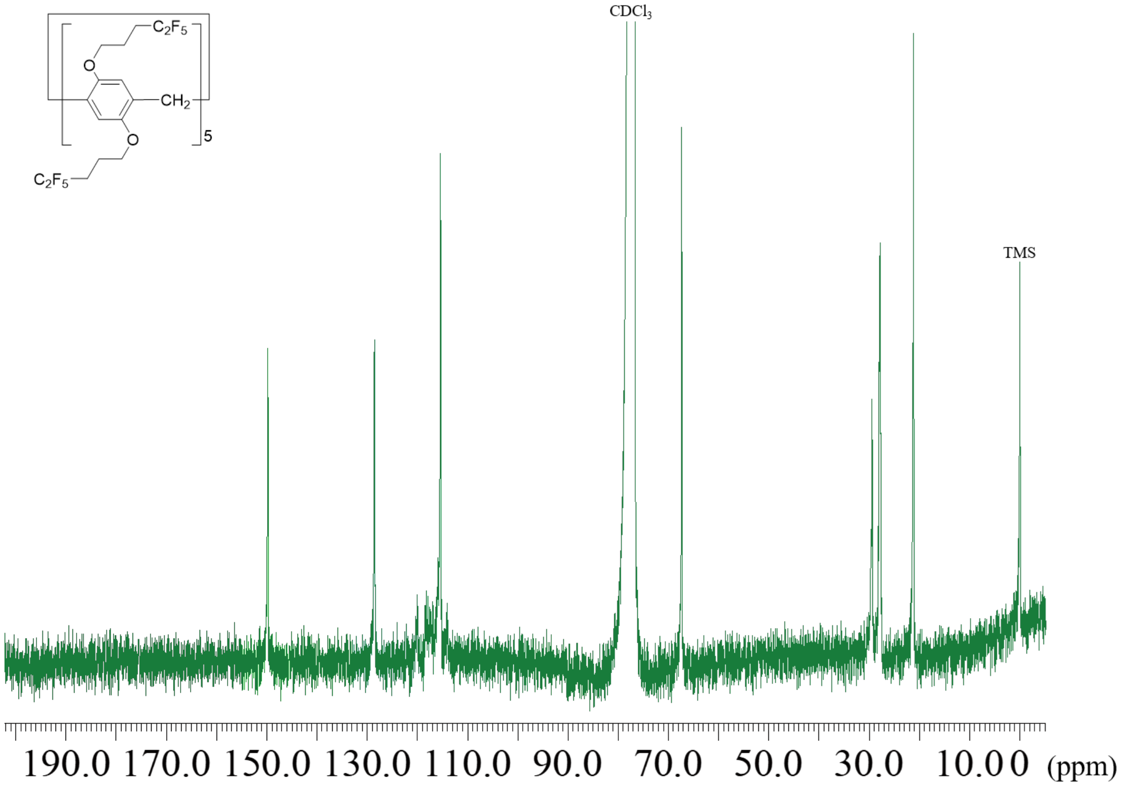


**Fig. S2** $^{13}$C NMR spectrum of **F5** ($CDCl_3$, 25 °C).

Peaks from carbons covalently bonded with fluorine atoms were split multiply in the range of 114.0–122.2 ppm due to the strong $^{13}$C-$^{19}$F coupling. Undulations in the baseline were due to use of cold probe (ECZ600) and difficult to adjust.

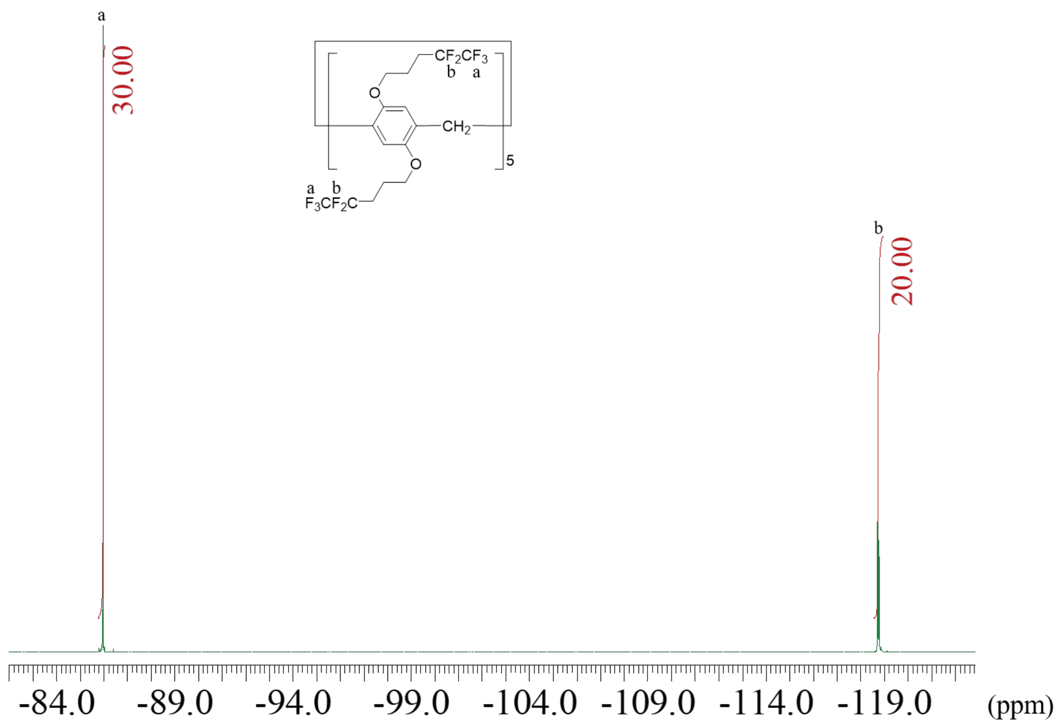


**Fig. S3** $^{19}$F NMR spectrum of **F5** ($CDCl_3$, 25 °C).

**F3**. To a flask containing pillar[5]arene with 10 hydroxyl groups (0.650 g, 1.07 mmol) was added dry DMF (15 mL), dry THF (15 mL) and NaH (0.830 g, 33.4 mmol). The resulting mixture was stirred at 60 °C for 72 h under a nitrogen atmosphere where after 4,4,4-trifluorobutyl 4-methylbenzenesulfonate[S3] (6.05 g, 21.5 mmol) was added. The reaction mixture was quenched with methanol, washed with brine, and dried over anhydrous $Na_2SO_4$. After filtration, the solvent was evaporated under reduced pressure. Column chromatography (silica gel; *n*-hexane:DCM = 2:1) afforded a white solid (276 mg, 0.161 mmol, yield 15%).

**Scheme S2** Synthesis of **F3**.

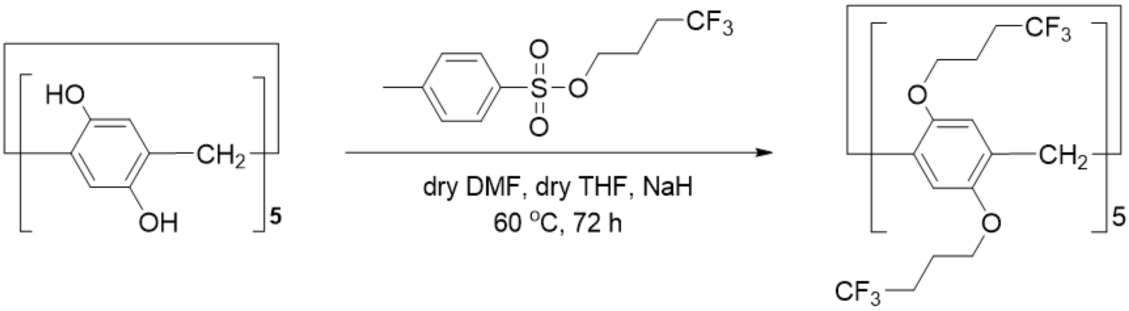


$^1$H NMR (**Fig. S4**, 400 MHz, $CDCl_3$, 25 °C) δ 6.75 (s, 10H), 3.89 (t, $J$ = 10.8 Hz, 20H), 3.74 (s, 10H), 2.29–2.41 (m, 20H), 2.01–2.08 (m, 20H); $^{13}$C NMR (**Fig. S5**, 151 MHz, $CDCl_3$, 25 °C) δ 149.7, 128.4, 127.1 (q, $^1J_{C–F}$ = 276.1 Hz), 115.2, 66.8, 30.9 (q, $^2J_{C–F}$ = 29.4 Hz), 29.5, 22.6; $^{19}$F NMR (**Fig. S6**, 376 MHz, $CDCl_3$, 25 °C) δ −67.0; MS (APCI) calcd. for $C_{75}H_{81}O_{10}F_{30}$ $[M + H]^+$: 1177.5286, found 1177.5345.

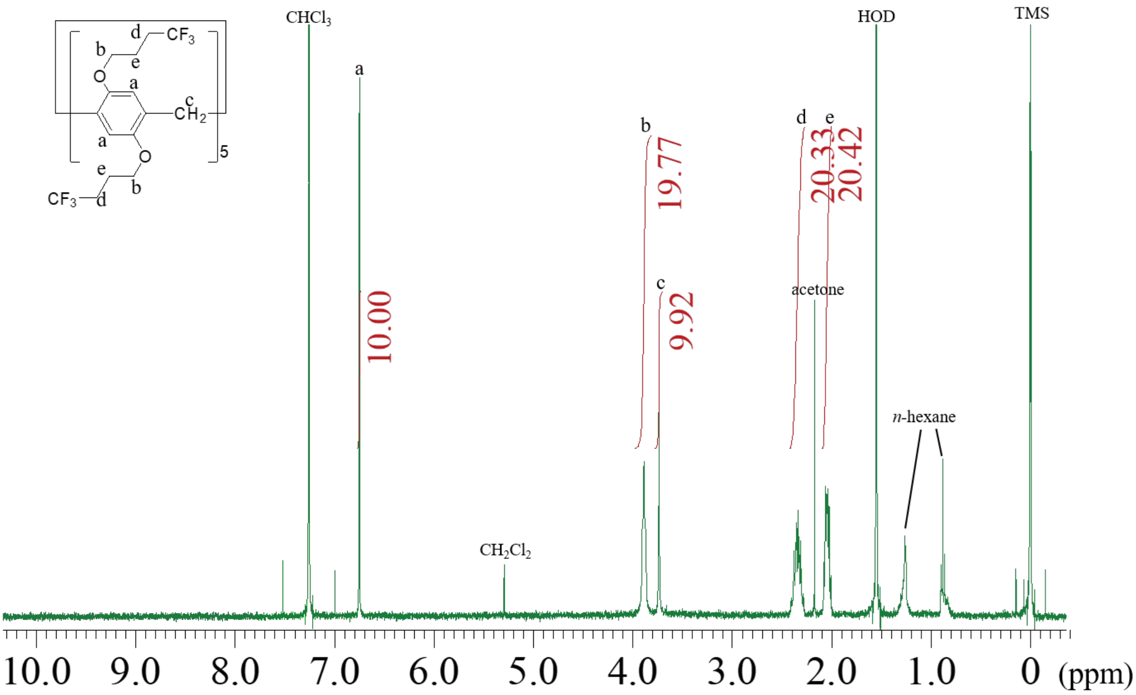


**Fig. S4** $^1$H NMR spectrum of **F3** ($CDCl_3$, 25 °C).

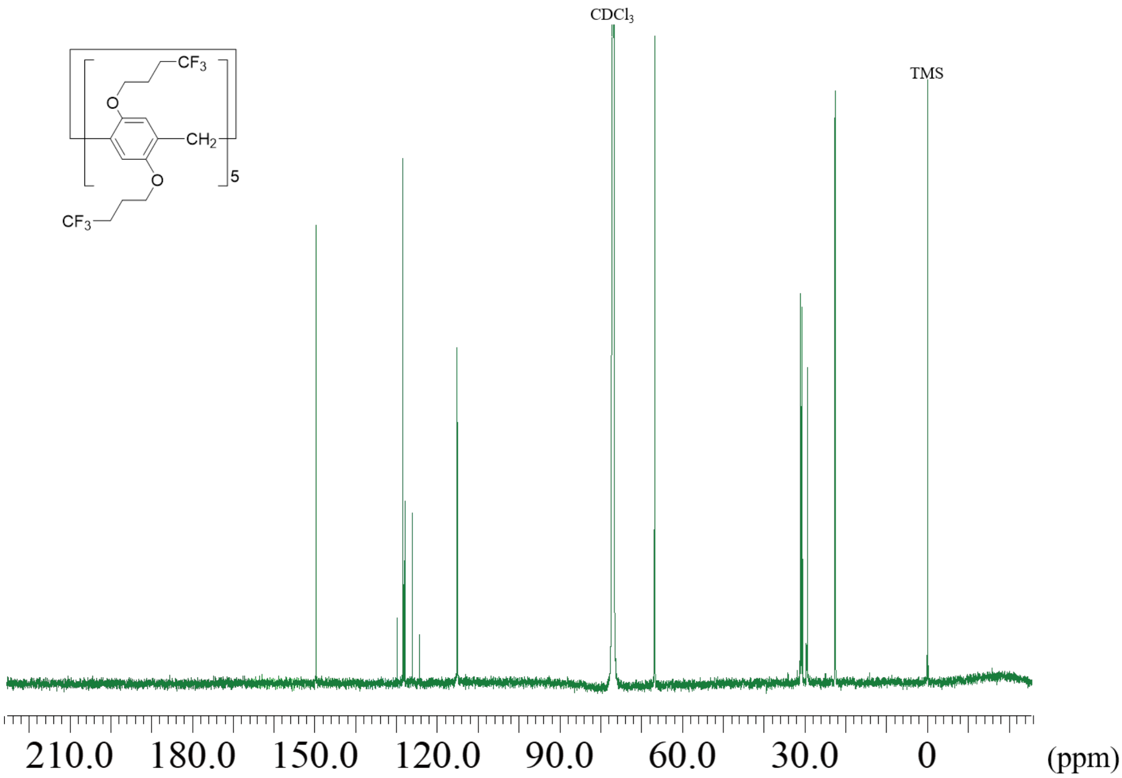


**Fig. S5** $^{13}C$ NMR spectrum of **F3** ($CDCl_3$, 25 °C).

Undulations in the baseline were due to use of cold probe (ECZ600) and difficult to adjust.

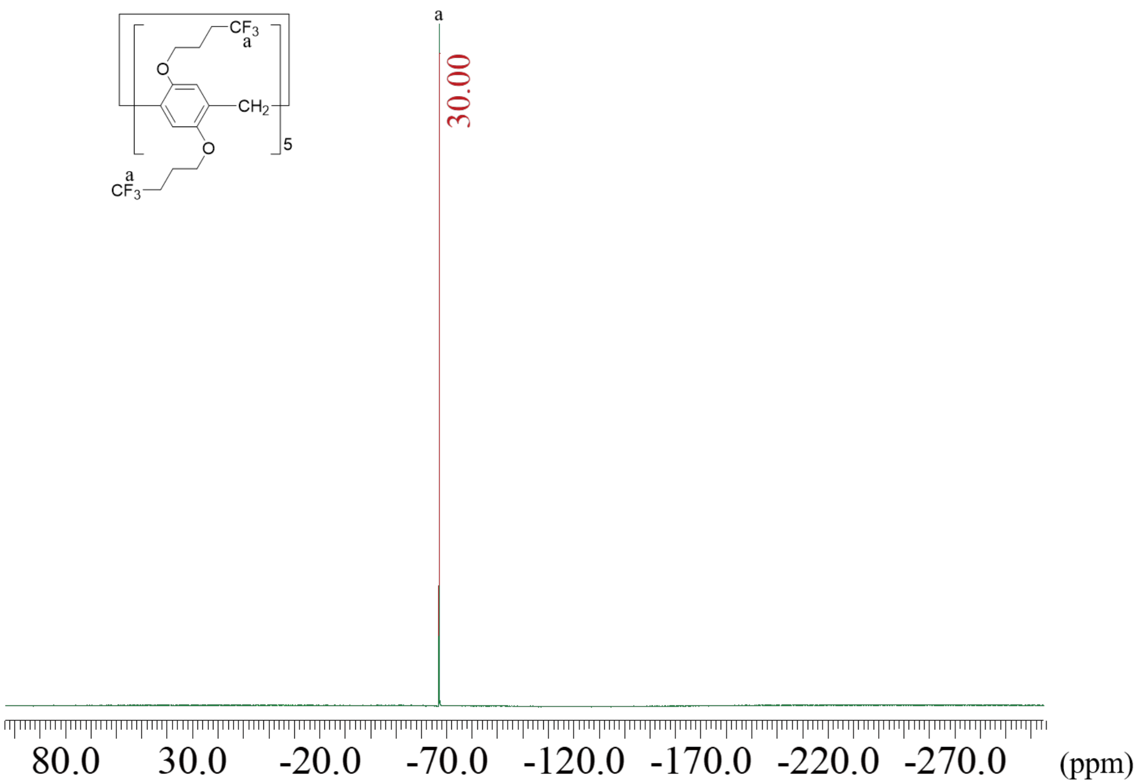


**Fig. S6** $^{19}F$ NMR spectrum of **F3** ($CDCl_3$, 25 °C).

**F13**. To a flask containing pillar[5]arene with 10 hydroxyl groups (0.650 g, 1.07 mmol) was added dry DMF (15 mL), dry THF (15 mL) and NaH (0.830 g, 33.4 mmol). The resulting mixture was stirred at 60 °C for 72 h under a nitrogen atmosphere where after compound **A**[S5] (11.3 g, 21.5 mmol) was added. The reaction mixture was quenched with methanol, washed with brine, and dried over anhydrous $Na_2SO_4$. After filtration, the solvent was evaporated under reduced pressure. Gel permeation chromatography afforded a brown solid (288 mg, 0.0567 mmol, yield 5.3%).

**Scheme S3** Synthesis of **F13**.

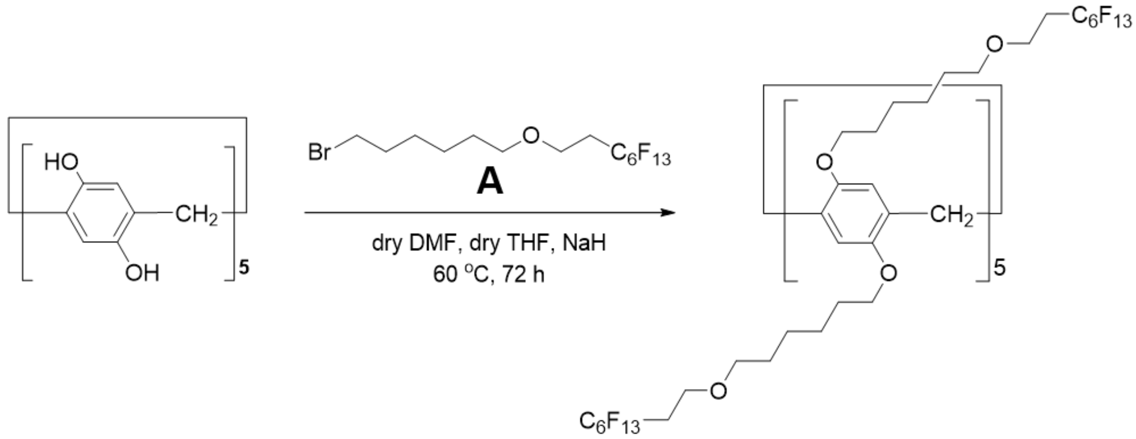


$^{1}$H NMR (**Fig. S7**, 400 MHz, $CDCl_3$, 25 °C) δ 6.83 (bs, 10H), 2.85–4.69 (m, 90H), 2.36 (bs, 19H), 1.71–2.15 (m, 30H), 1.45 (bs, 29H); $^{13}$C NMR (**Fig. S8**, 151 MHz, $CDCl_3$, 25 °C) δ 149.8, 128.2, 105.3–120.1, 71.2, 68.0, 62.5, 33.9, 32.7, 31.5, 29.6, 26.1, 22.7; $^{19}$F NMR (**Fig. S9**, 376 MHz, $CDCl_3$, 25 °C) δ −81.3, −114.2, −122.6, −123.6, −124.3, −126.8. MS could not be measured as **F13** with long $C_6F_{13}$ groups was high molecular weight compound and difficult to ionize.

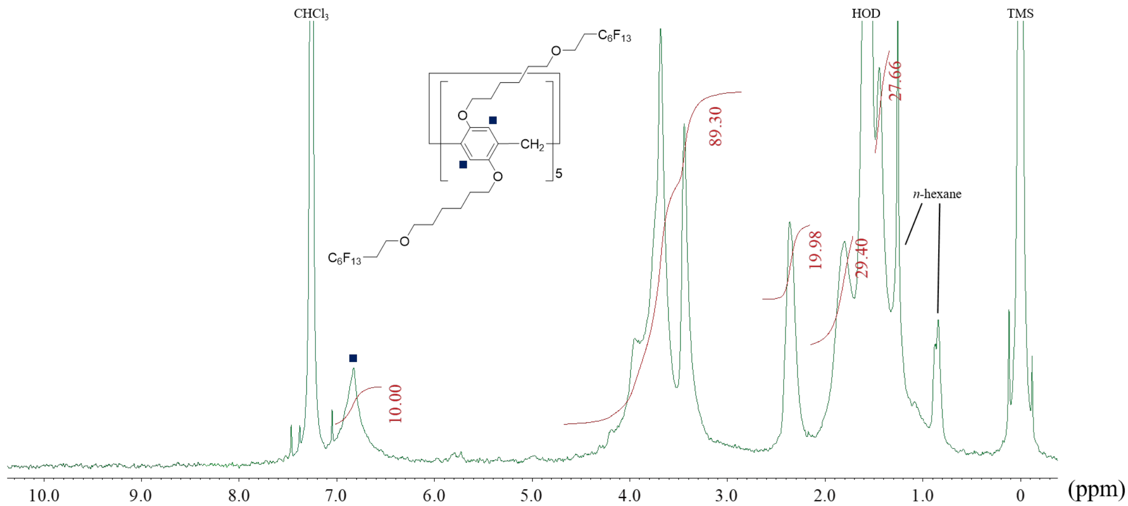


**Fig. S7** $^{1}$H NMR spectrum of **F13** ($CDCl_3$, 25 °C).

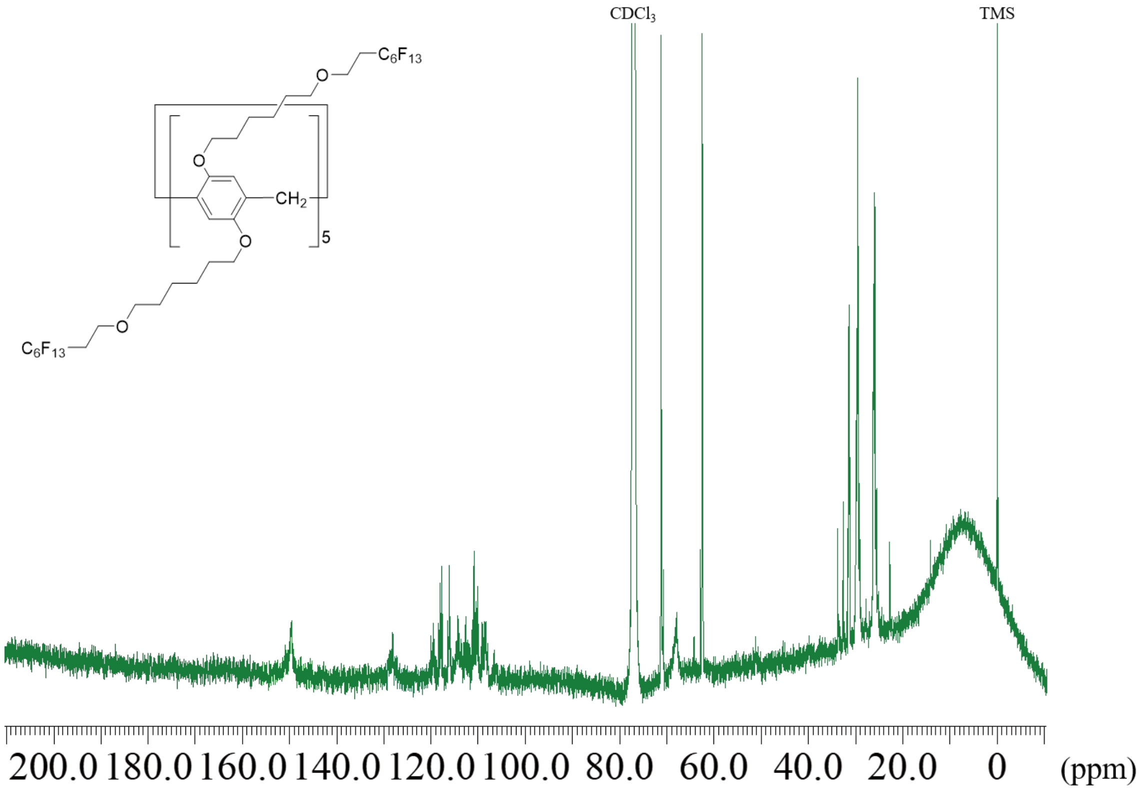

**Fig. S8** $^{13}$C NMR spectrum of **F13** ($CDCl_3$, 25 °C).

Peaks from carbons covalently bonded with fluorine atoms were split multiply in the range of 105.3–120.1 ppm due to the strong $^{13}$C-$^{19}$F coupling. Undulations in the baseline were due to use of cold probe (ECZ600) and difficult to adjust.

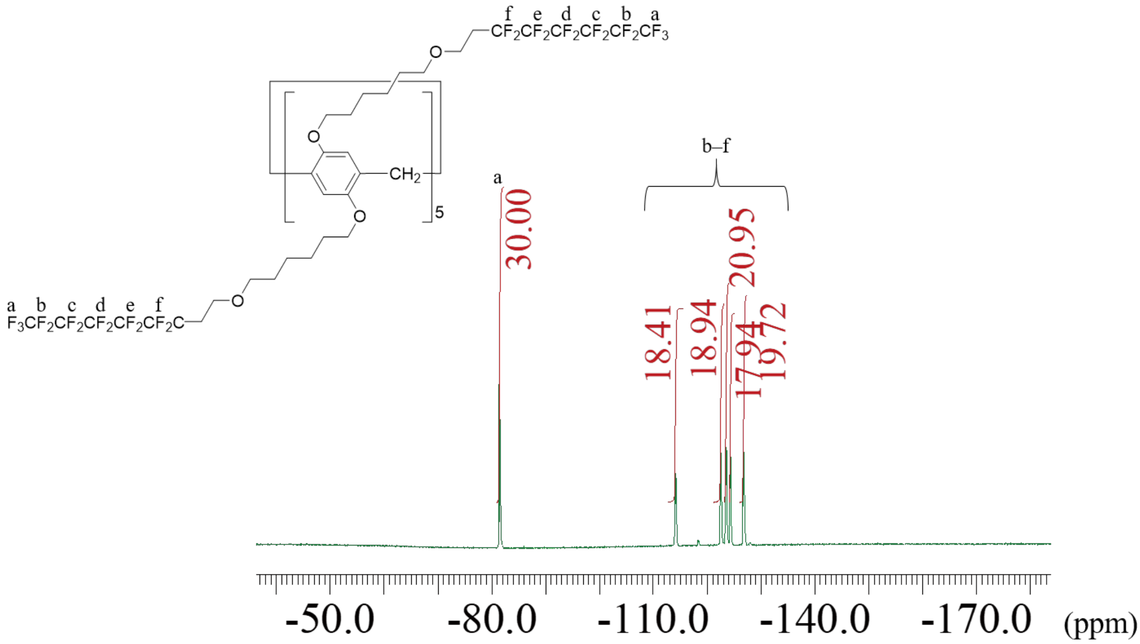


**Fig. S9** $^{19}$F NMR spectrum of **F13** ($CDCl_3$, 25 °C).

**Monomer Unit**. To a flask containing hydroquinone (1.10 g, 10.0 mmol) was added acetonitrile (33.3 mL) and $K_2CO_3$ (4.14 g, 30.0 mmol). The resulting mixture was stirred at 95 °C for 24 h where after 4,4,5,5,5-pentafluoropentyl 4-methylbenzenesulfonate[S3] (6.65 g, 20.0 mmol) was added. The reaction mixture was washed with water, and dried over anhydrous $Na_2SO_4$. After filtration, the solvent was evaporated under reduced pressure. Column chromatography (silica gel; *n*-hexane:DCM = 2:1) afforded a white solid (3.51 g, 8.15 mmol, yield 82%).

**Scheme S4** Synthesis of **Monomer Unit**.

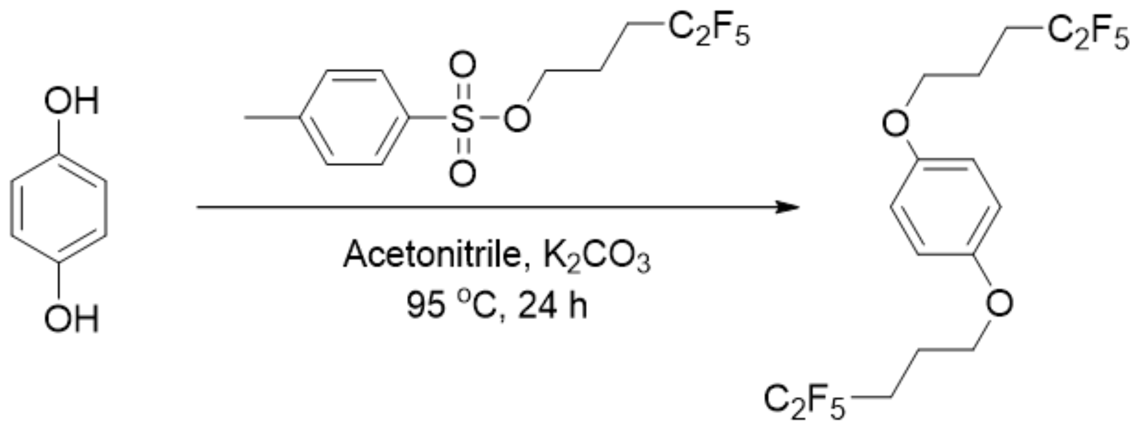


$^1$H NMR (**Fig. S10**, 400 MHz, $CDCl_3$, 25 °C) δ 6.83 (s, 4H), 3.98 (t, $J$ = 6.0 Hz, 4H), 2.20-2.33 (m, 4H), 2.03-2.09 (m, 4H); $^{13}$C NMR (**Fig. S11**, 151 MHz, $CDCl_3$, 25 °C) δ 153.0, 119.2 (qt, $^1J_{C–F}$ = 286.9 Hz, $^2J_{C–F}$ = 37.8 Hz), 115.9 (tq, $^1J_{C–F}$ = 252.9 Hz, $^2J_{C–F}$ = 37.8 Hz), 115.5, 113.8–122.3, 66.9, 27.7, 20.8; $^{19}$F NMR (**Fig. S12**, 376 MHz, $CDCl_3$, 25 °C) δ −85.9, −118.8; HR-MS (EI) calcd. for $C_{16}H_{16}O_2F_{10}$ $[M]^+$: 430.0986, found 430.0989.

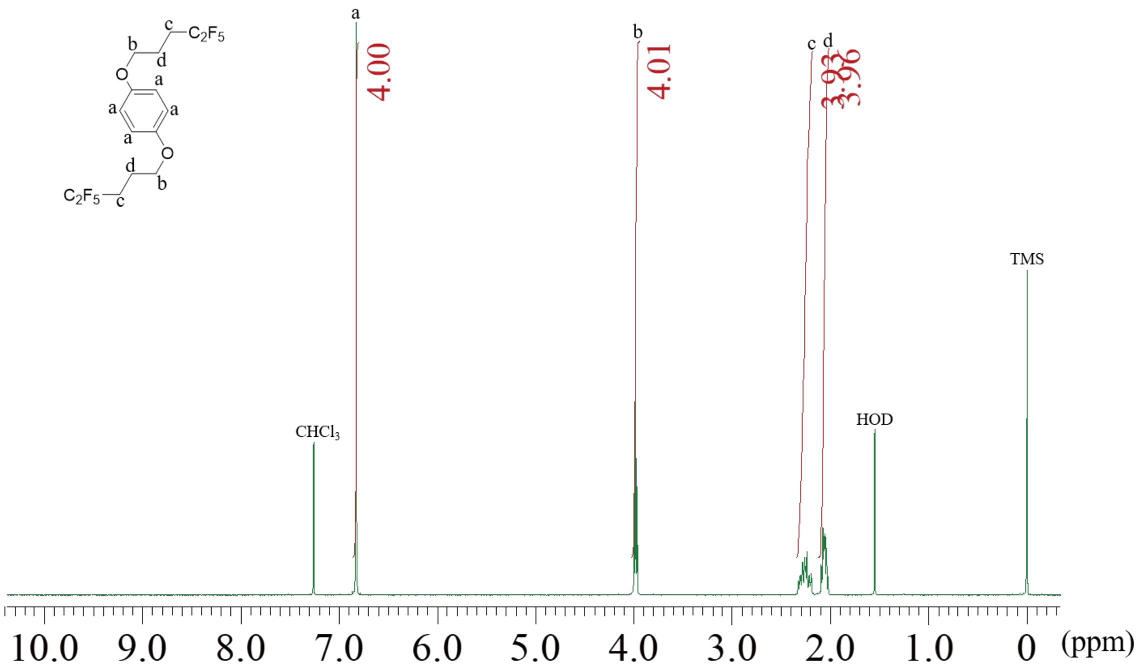


**Fig. S10** $^1$H NMR spectrum of **Monomer Unit** ($CDCl_3$, 25 °C).

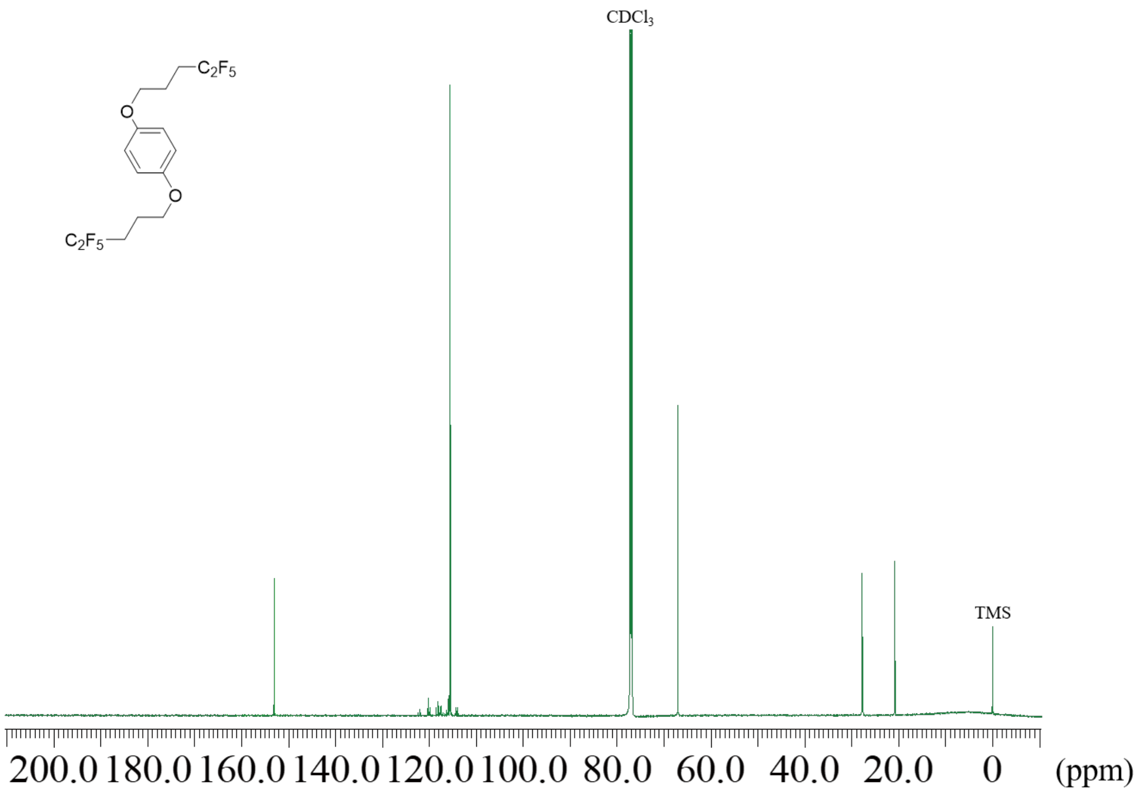


**Fig. S11** $^{13}$C NMR spectrum of **Monomer Unit** ($CDCl_3$, 25 °C).

Undulations in the baseline were due to use of cold probe (ECZ600) and difficult to adjust.

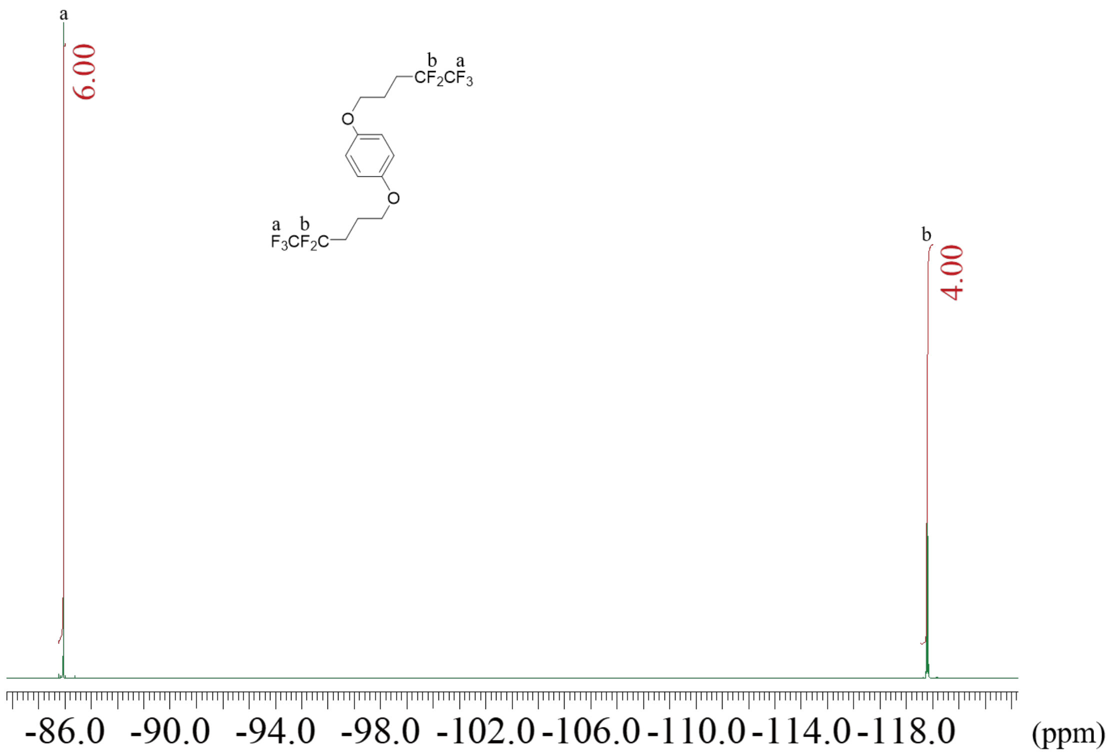


**Fig. S12** $^{19}$F NMR spectrum of **Monomer Unit** ($CDCl_3$, 25 °C).

**C5P[5]A**. This compound was synthesized according to the previous paper.[S6]

**[6]F5**. To a flask containing pillar[6]arene with 12 hydroxyl groups (0.650 g, 0.885 mmol) was added dry DMF (15 mL), dry THF (15 mL) and NaH (0.830 g, 33.4 mmol). The resulting mixture was stirred at 60 °C for 72 h under a nitrogen atmosphere where after 4,4,5,5,5-pentafluoropentyl 4-methylbenzenesulfonate[S3] (7.15 g, 21.5 mmol) was added. The reaction mixture was quenched with methanol, washed with brine, and dried over anhydrous $Na_2SO_4$. After filtration, the solvent was evaporated under reduced pressure. Column chromatography (silica gel; *n*-hexane:DCM = 4:1) afforded a white solid (569 mg, 0.214 mmol, yield 24%).

**Scheme S5** Synthesis of **[6]F5**.

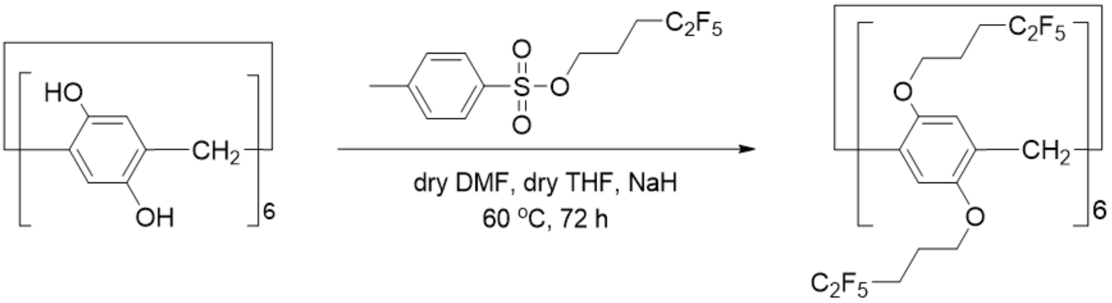


$^1$H NMR (**Fig. S13**, 400 MHz, $CDCl_3$, 25 °C) δ 6.66 (s, 12H), 3.78–3.82 (m, 36H), 2.14–2.27 (m, 24H), 1.93–2.00 (m, 24H); $^{13}$C NMR (**Fig. S14**, 151 MHz, $CDCl_3$, 25 °C) δ 150.3, 128.1, 115.0, 112.5–120.5, 67.1, 29.7, 27.7, 20.9; $^{19}$F NMR (**Fig. S15**, 376 MHz, $CDCl_3$, 25 °C) δ −86.1, −118.9; MS (APCI) calcd. for $C_{102}H_{97}O_{12}F_{60}$ $[M + H]^+$: 2653.5984, found 2654.5982.

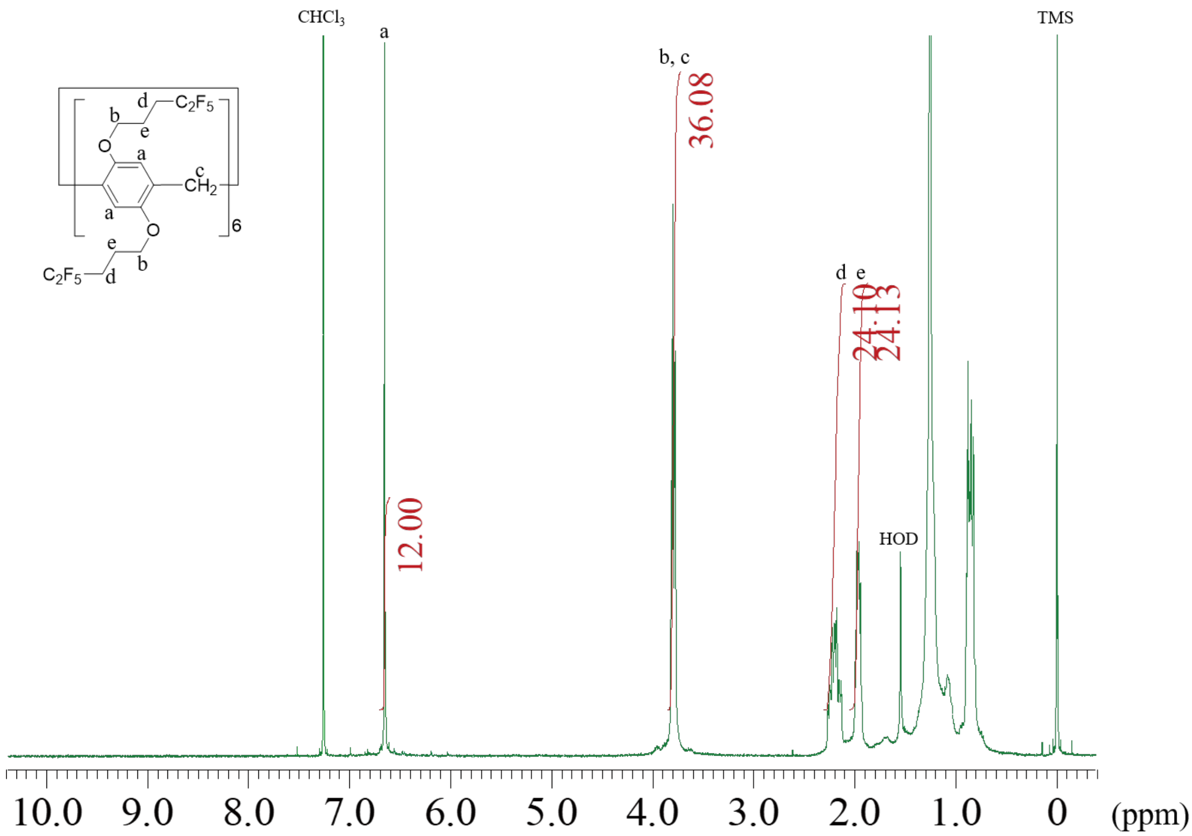


**Fig. S13** $^1$H NMR spectrum of **[6]F5** ($CDCl_3$, 25 °C).

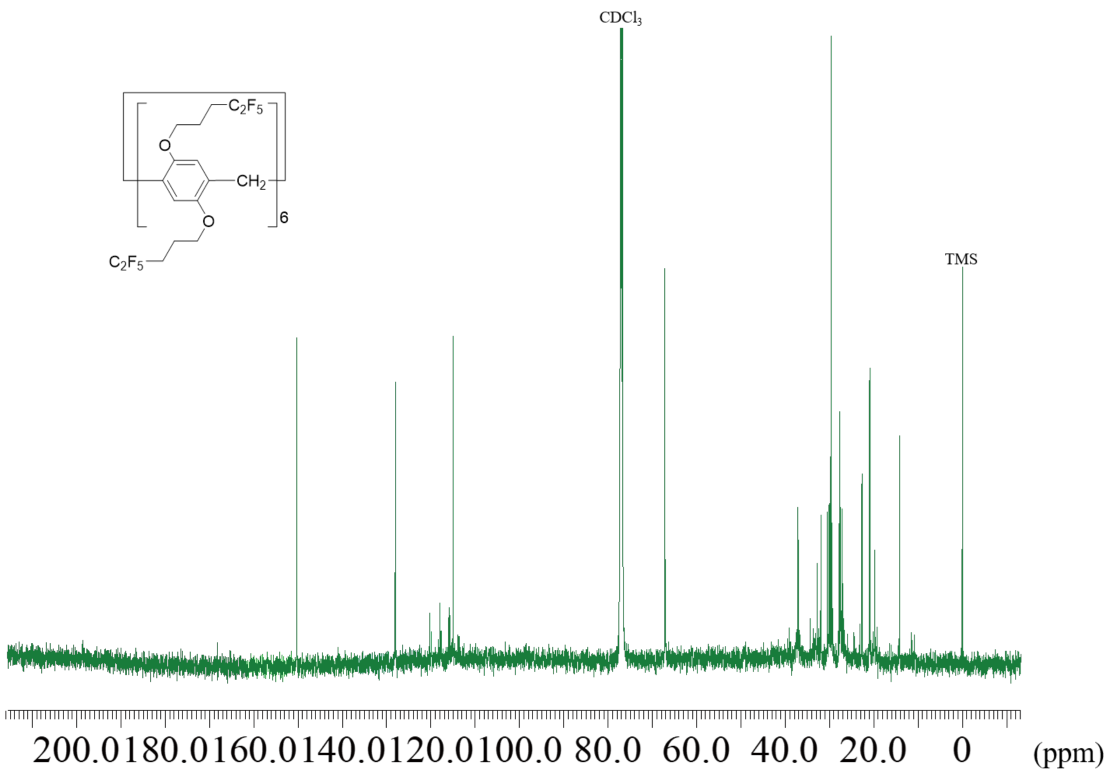


**Fig. S14** $^{13}$C NMR spectrum of **[6]F5** (CDCl$_3$, 25 °C).

Peaks from carbons covalently bonded with fluorine atoms were split multiply in the range of 112.5–120.5 ppm due to the strong $^{13}$C-$^{19}$F coupling. Undulations in the baseline were due to use of cold probe (ECZ600) and difficult to adjust.

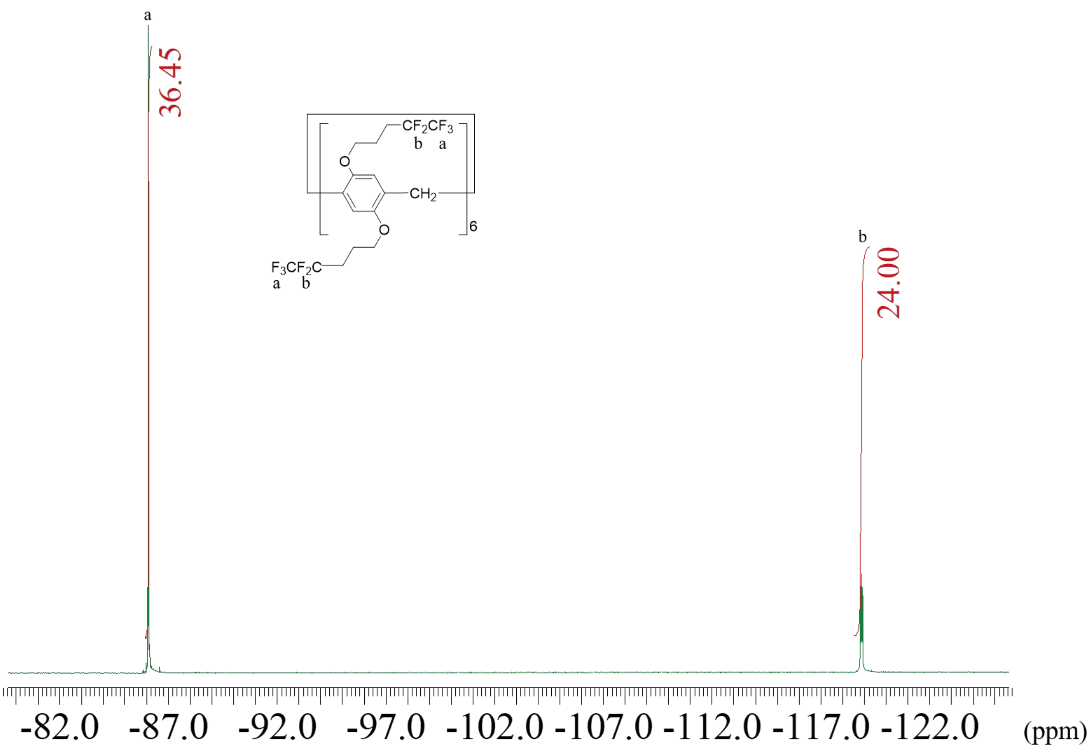


**Fig. S15** $^{19}$F NMR spectrum of **[6]F5** (CDCl$_3$, 25 °C).

## 3. Phase changes of F5 and reference compounds

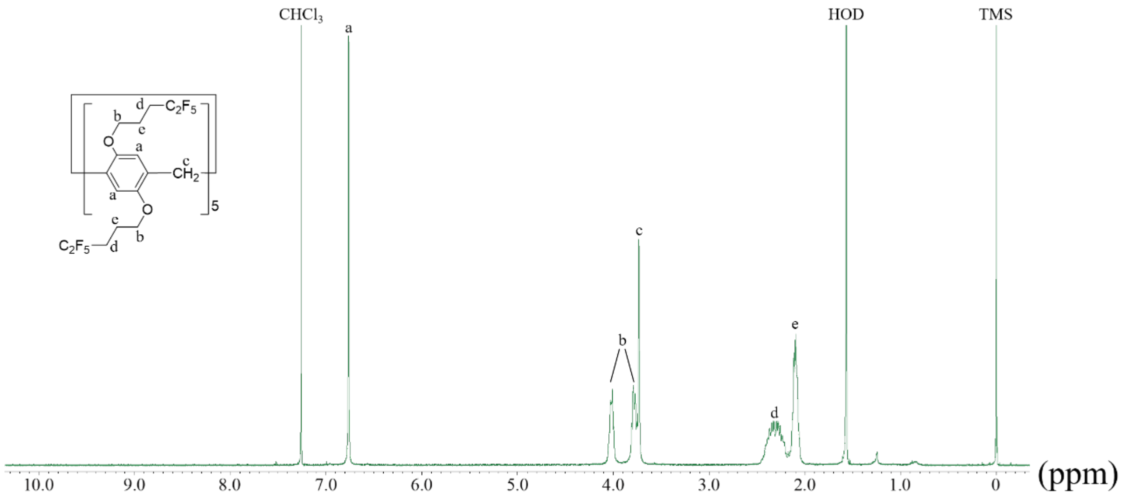


**Fig. S16** $^{1}$H NMR spectrum of ***c*-F5** ($CDCl_3$, 25 °C).

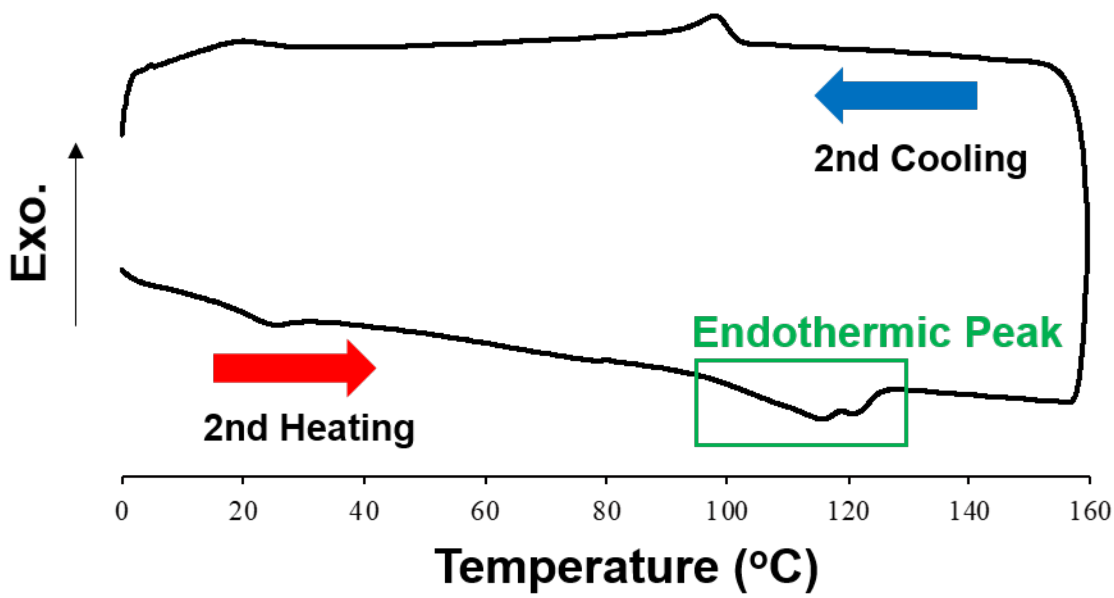


**Fig. S17** DSC second heating and cooling curve of ***c*-F5** (scanning rate: 10 °C/min).

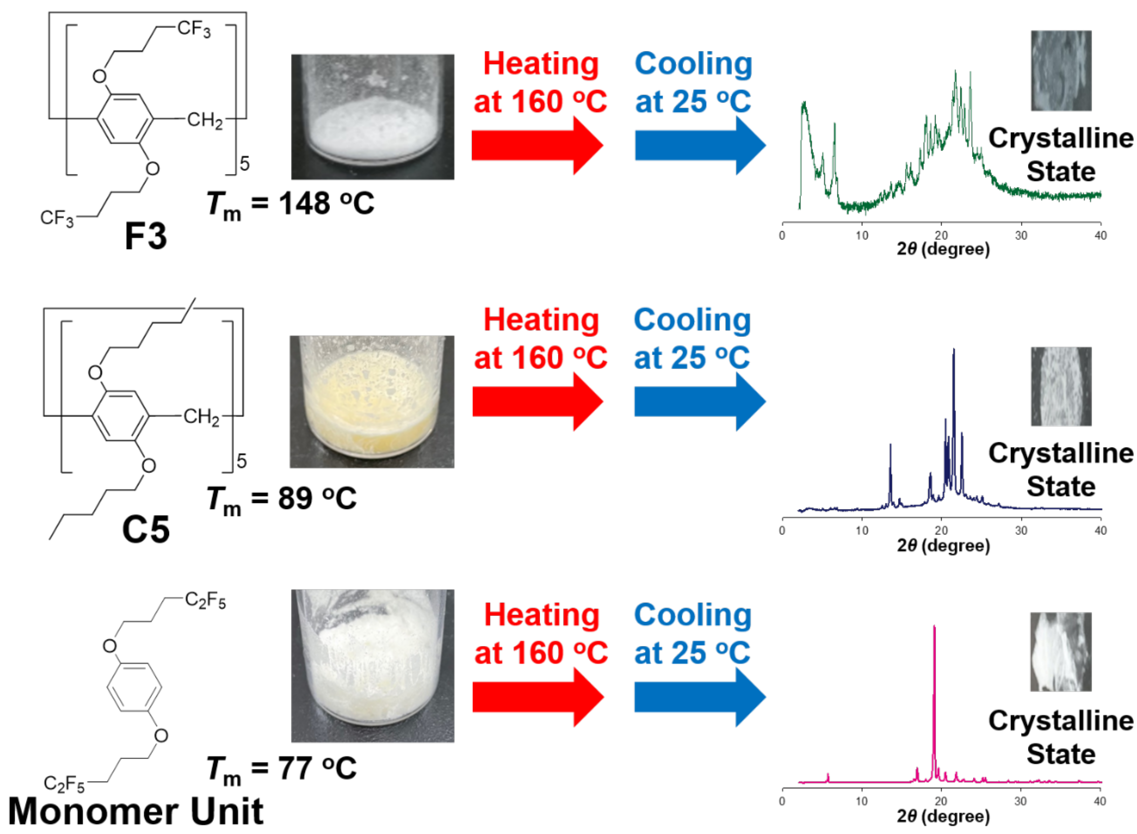


**Fig. S18** Photographs and PXRD patterns of **F3** (top), **C5** (middle) and **Monomer Unit** (bottom) before (left) and after (right) heating over melting points and then cooling at 25 °C.

From PXRD measurements, all of the resulting samples after cooling showed sharp diffraction peaks, indicating crystalline to liquid phase change by heating, and liquid to crystalline phase change by cooling. These transitions are normal in low molecular weight organic compounds including typical pillar[n]arenes.[S7-S9]

(a)

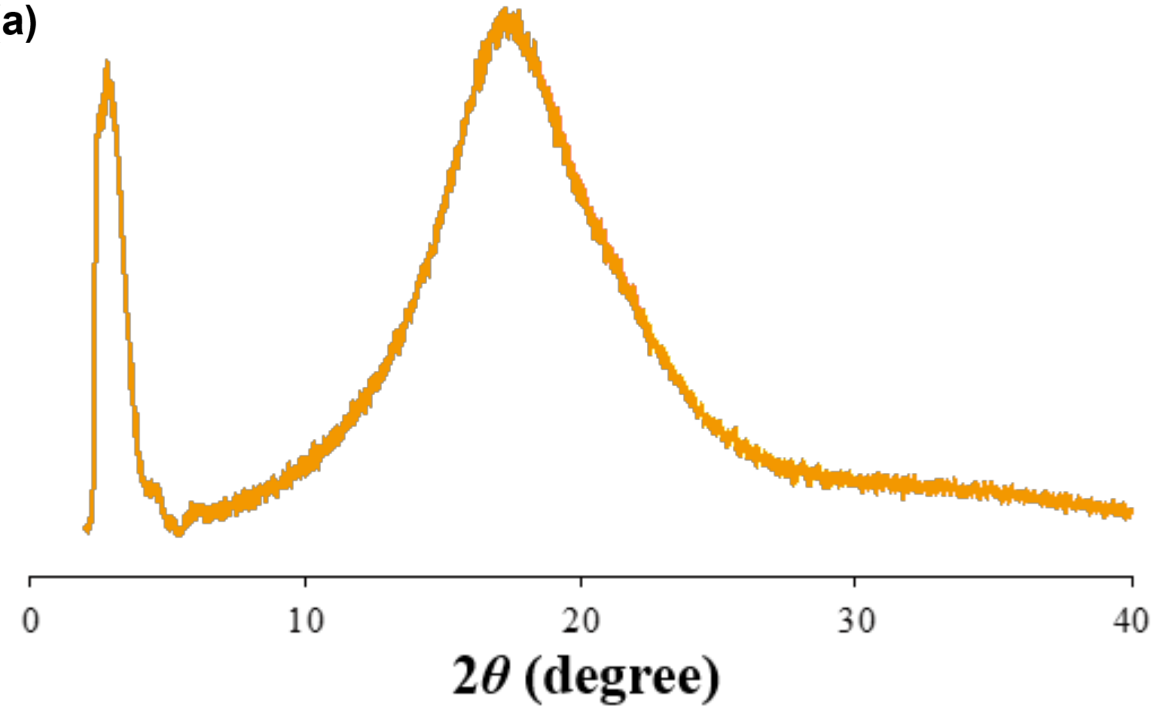

0
10
20
30
40
2θ (degree)


(b)

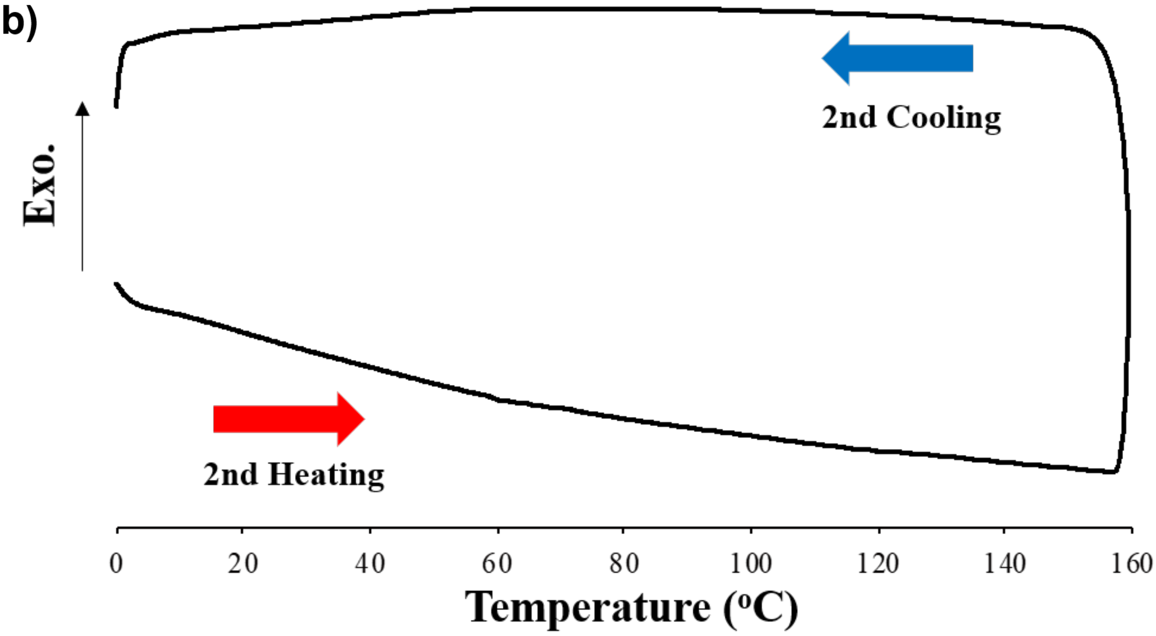

Exo.
2nd Cooling
2nd Heating
0
20
40
60
80
100
120
140
160
Temperature (°C)

(c)

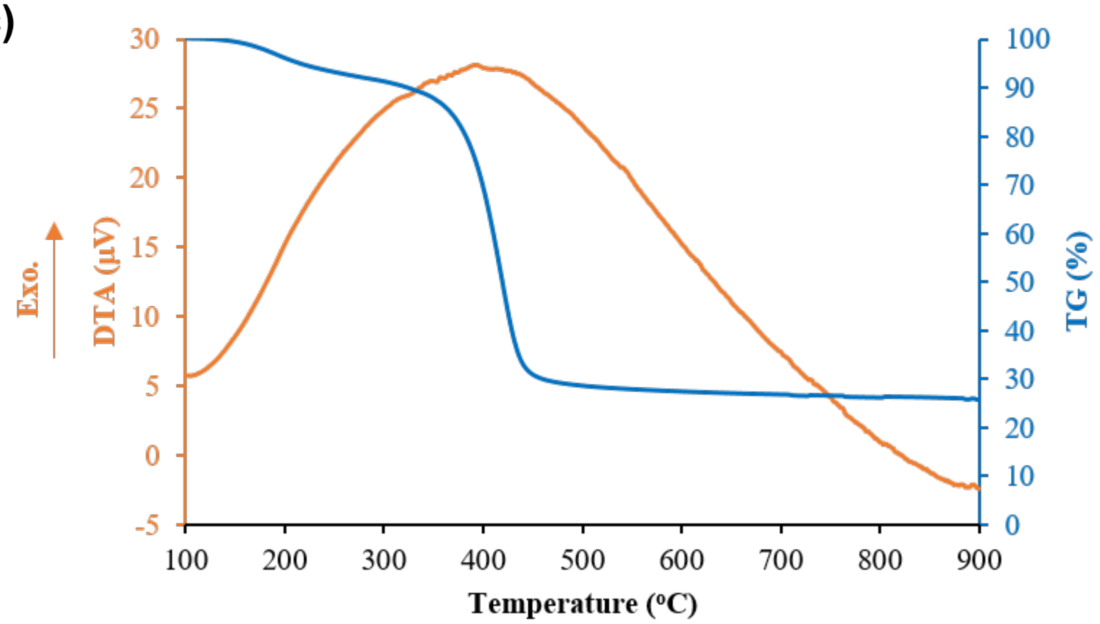


**Fig. S19** (a) PXRD pattern, (b) DSC second heating and cooling curve and (c) TG-DTA traces of **F13** (scanning rates of DSC and TD-DTA: 10 °C/min).

PXRD pattern suggested that **F13** existed in an amorphous state at 25 ºC. From DSC measurement, there was no endothermic peak until 160 ºC, indicating no melting until 160 ºC. From TG-DTA measurement, a broad exothermic peak from about 300 to 600 °C and weight loss at about 400 °C were observed, suggesting decomposition of **F13** over 300 ºC. These results indicate that **F13** did not show an amorphous–crystalline transition as **F5** did.

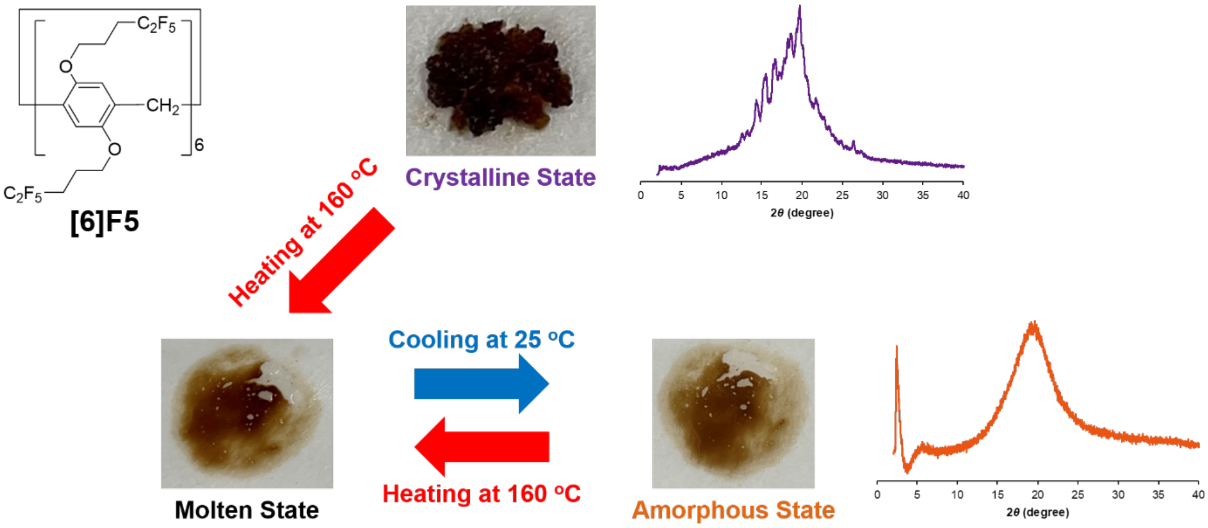


**Fig. S20** Photographs and PXRD patterns of **[6]F5** before and after heating over melting points and then cooling at 25 °C.

From PXRD measurements, the resulting sample after cooling did not show sharp diffraction peaks, while the sample before heating showed sharp diffraction peaks, indicating the crystalline to amorphous phase change as **F5** did. From this result, $C_2F_5$ groups are good substituents for the formation of the molecular glasses.

**4. State and contact angle changes by *n*-hexane vapor**

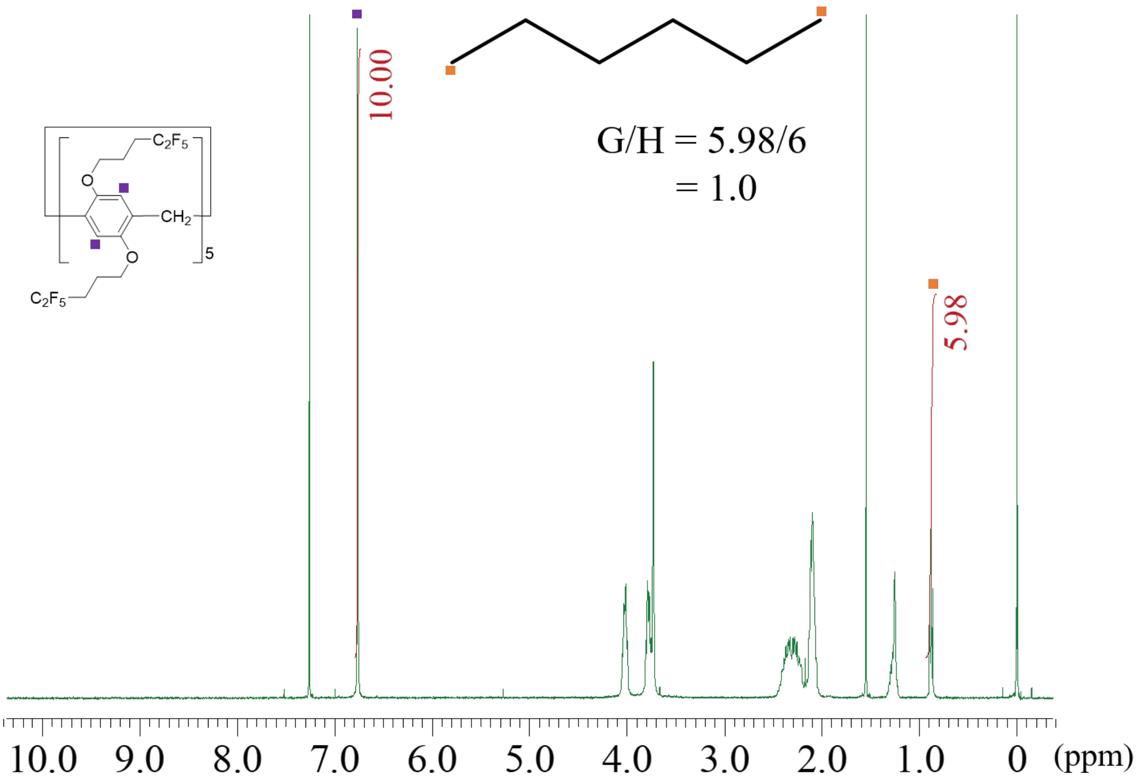


**Fig. S21** $^{1}$H NMR spectrum of ***c*-(F5⊃H)** ($CDCl_3$, 25 °C). The uptake ratio of *n*-hexane to **F5** (G/H) calculated from the integration ratio was 1.0.

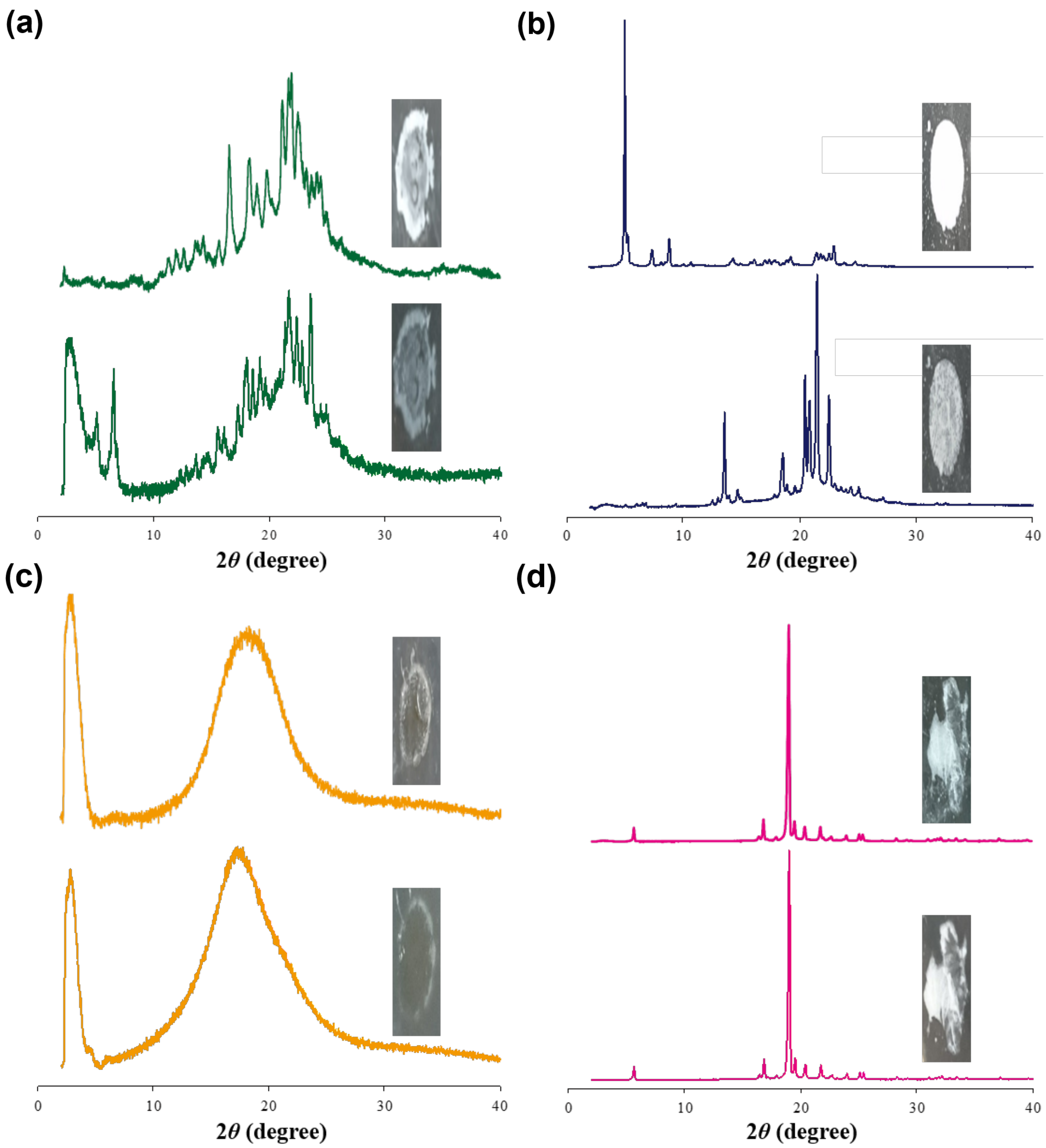


**Fig. S22** Photographs and PXRD patterns of (a) **F3**, (b) **C5**, (c) **F13** and (d) **Monomer Unit** before (lower side) and after (upper side) exposure to *n*-hexane vapor.

PXRD measurements of **F3** and **C5** showed sharp diffraction peaks in the samples before and after the vapor exposure, indicating that the samples before and vapor exposure were crystalline states. On the other hand, PXRD measurements of **F13** films both before and after exposure to the vapor showed no sharp peaks, suggesting that **F13** was an amorphous state even by the vapor treatment. In addition, PXRD patterns of **Monomer Unit** suggested that **Monomer Unit** remained in a crystalline state both before and after exposure to *n*-hexane vapor as it has no macrocyclic structure and did not take up *n*-hexane vapor. From these results, installation of the $C_2F_5$ groups into pillar[5]arene enabled the transition from amorphous to crystalline states by uptake of *n*-hexane vapor while no noticeable state transitions were observed in the other reference compounds by exposure to *n*-hexane vapor.

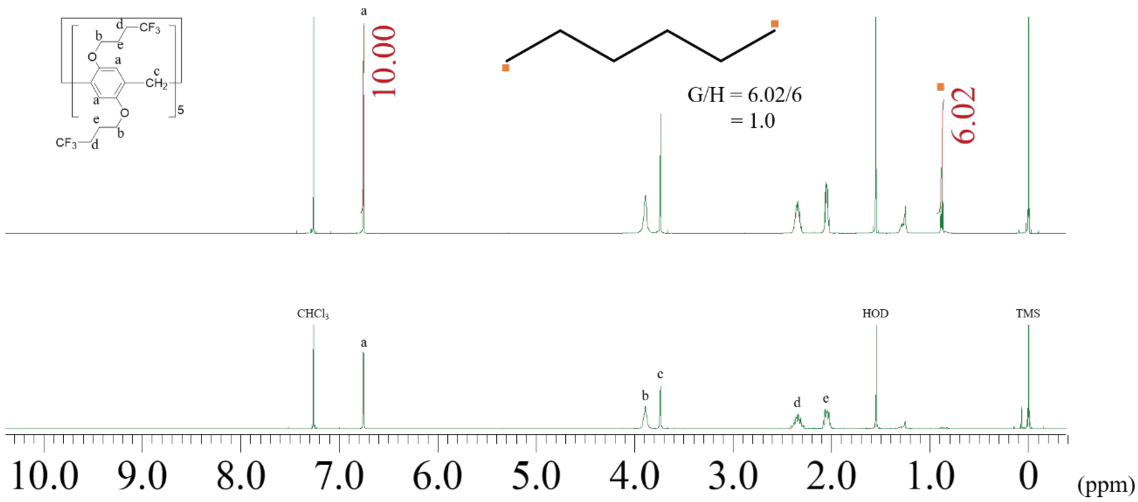


**Fig. S23** [1]H NMR spectra of **F3** ($CDCl_3$, 25 °C) before (lower side) and after (upper side) exposure to *n*-hexane vapor. The uptake ratio of *n*-hexane to **F3** (G/H) calculated from the integration ratio was 1.0.

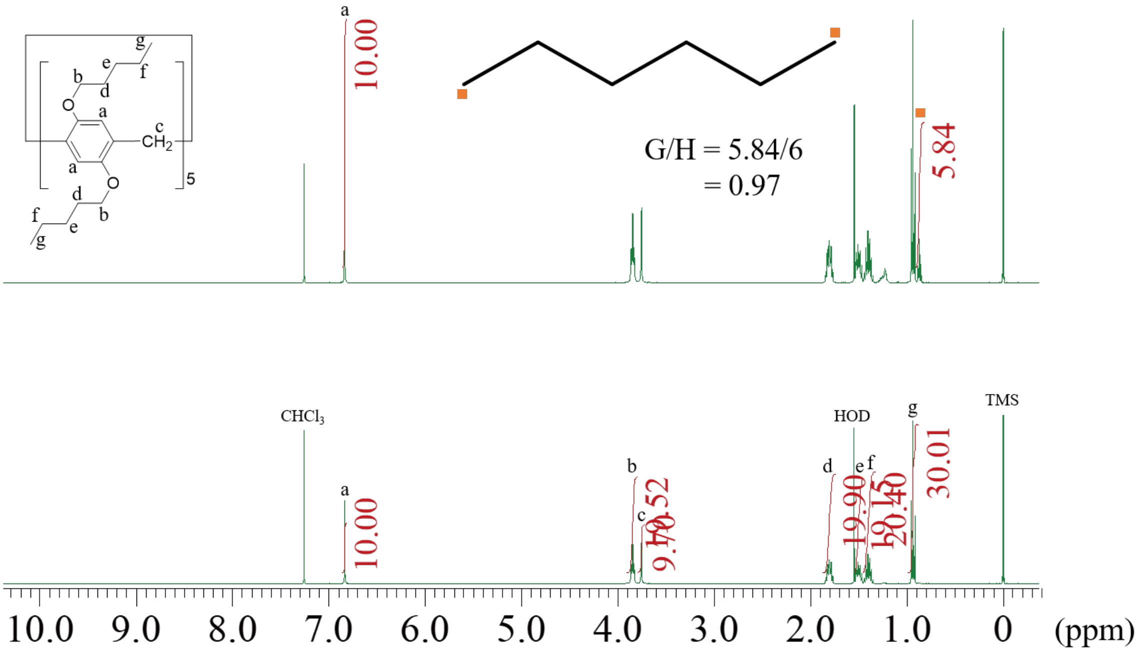


**Fig. S24** [1]H NMR spectra of **C5** ($CDCl_3$, 25 °C) before (lower side) and after (upper side) exposure to *n*-hexane vapor. The uptake ratio of *n*-hexane to **C5** (G/H) calculated from the integration ratio was 0.97.

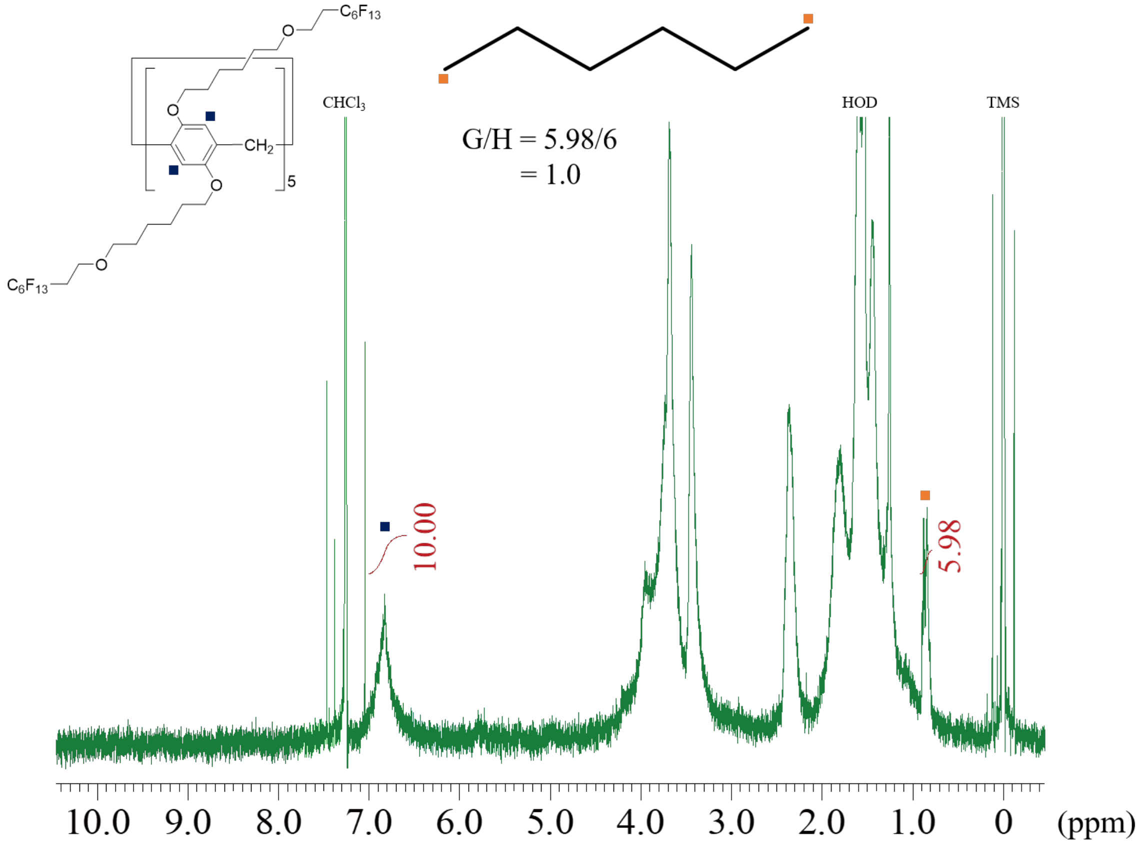


**Fig. S25** [1]H NMR spectrum of **F13** ($CDCl_3$, 25 °C) before exposure to *n*-hexane vapor. The ratio of *n*-hexane to **F13** (G/H) calculated from the integration ratio was 1.0.

Proton peaks from *n*-hexane were observed even after heating of **F13** as prepared at 200 °C in vacuo overnight, indicating that *n*-hexane used for the purification could not be removed from **F13** by the heating.

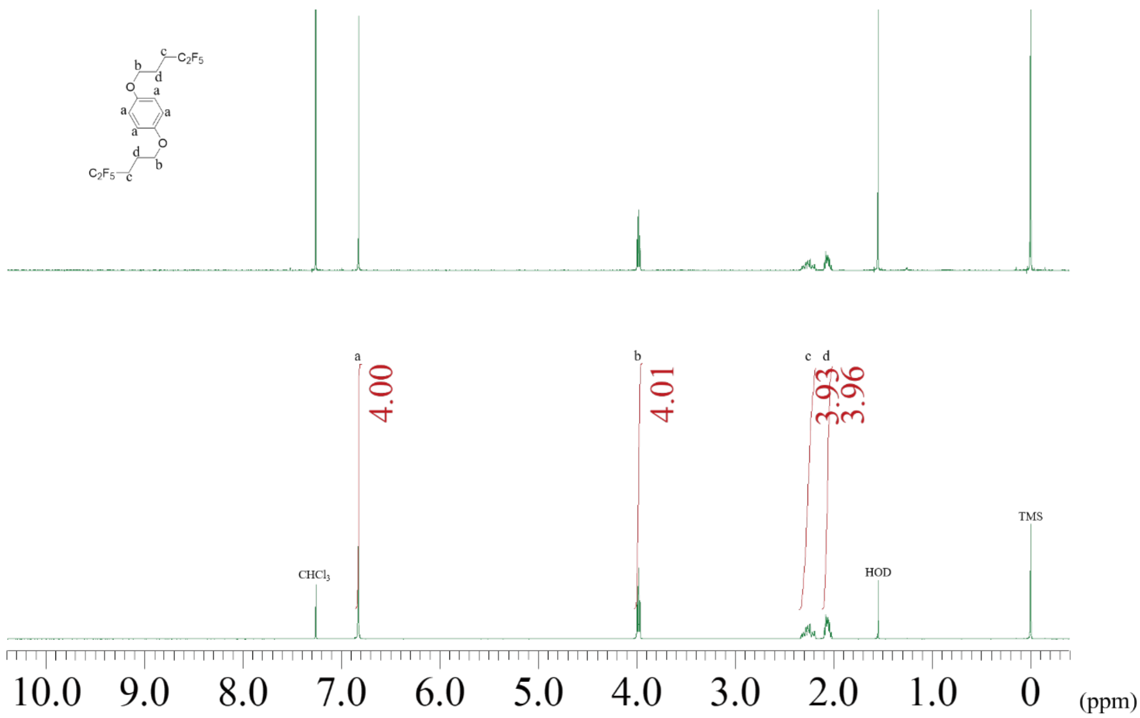


**Fig. S26** $^1$H NMR spectra of **Monomer Unit** ($CDCl_3$, 25 °C) before (lower side) and after (upper side) exposure to *n*-hexane vapor.

No proton signals from *n*-hexane after exposure to *n*-hexane vapor indicate that **Monomer Unit** with no macrocyclic structure did not take up *n*-hexane vapor.

**Table S1** Transmittance changes at 500 nm of **F5** by exposing ***a*-F5** to *n*-hexane vapor (odd times) and heating ***c*-(F5⊃H)** at 160 °C (even times).

| Times | Transmittance at 500 nm (%) |
|---|---|
| 1 | 98 |
| 2 | 10 |
| 3 | 95 |
| 4 | 8 |
| 5 | 94 |
| 6 | 3 |
| 7 | 90 |
| 8 | 14 |

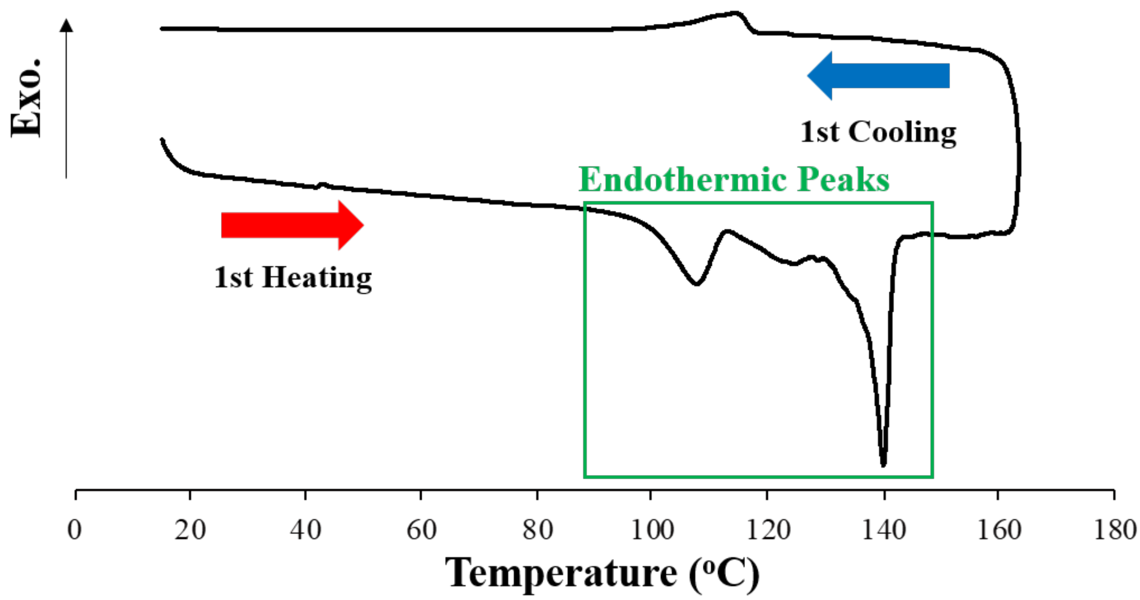


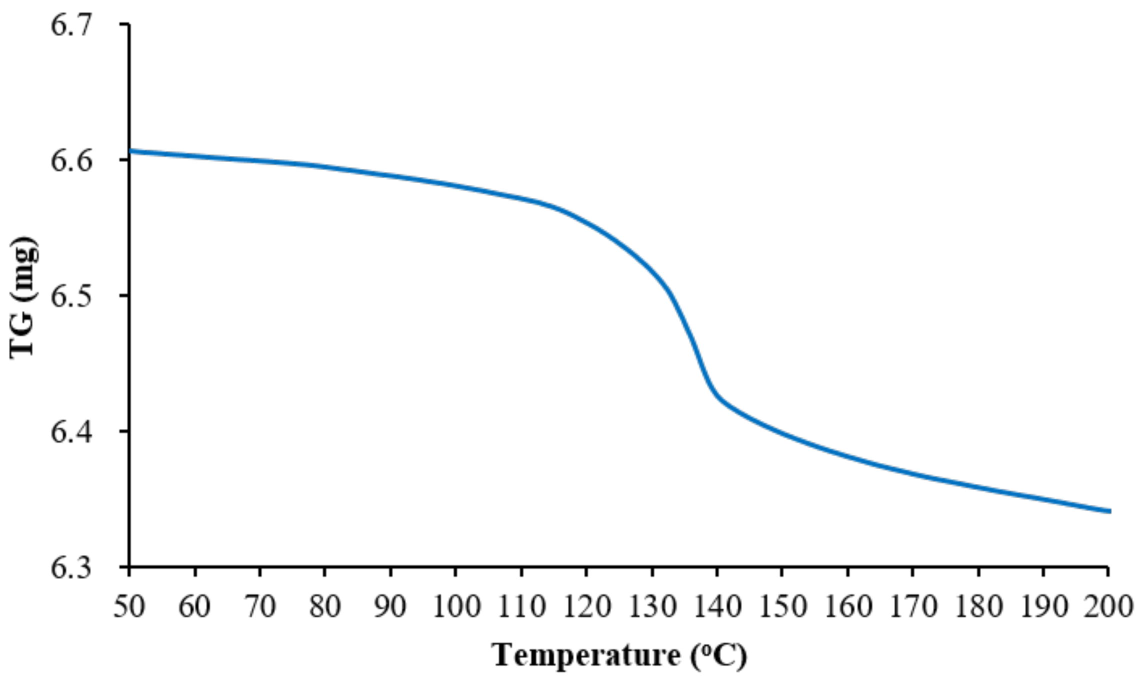


**Fig. S27** DSC first heating and cooling curve (upper side) and TG trace (lower side) of ***c*-(F5⊃H)** (scanning rates of DSC and TDA: 10 °C/min).

DSC curve showed two endothermic peaks at 108 and 140 °C. From TG trace, obvious weight loss was observed at around 140 °C, resulting from *n*-hexane release from ***c*-(F5⊃H)**. These results indicate that the peaks at lower and higher temperatures were attributed to the melting behavior of ***c*-(F5⊃H)** and the release of *n*-hexane, respectively.

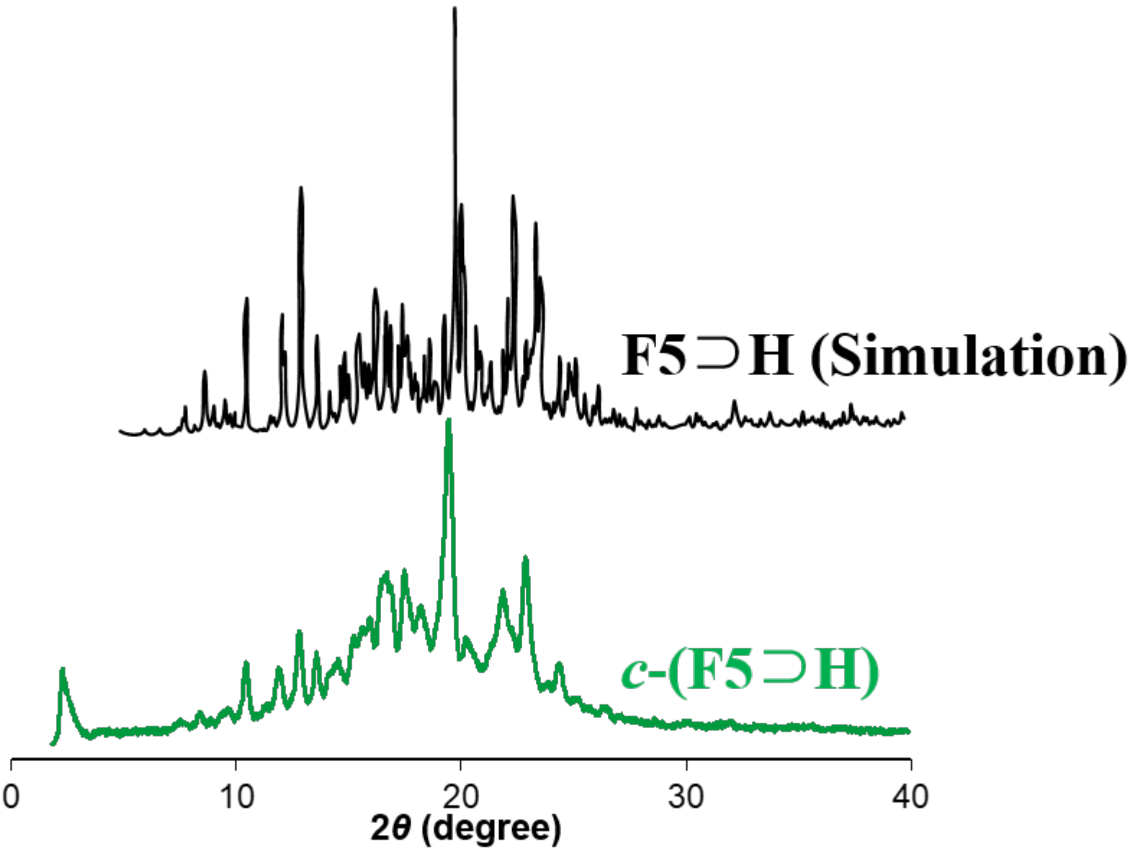


**Fig. S28** PXRD patterns of simulation from single crystal of **F5⊃H** (upper side) and ***c*-(F5⊃H)** (lower side).

## 5. Solid-state $^{13}C$ NMR spectra

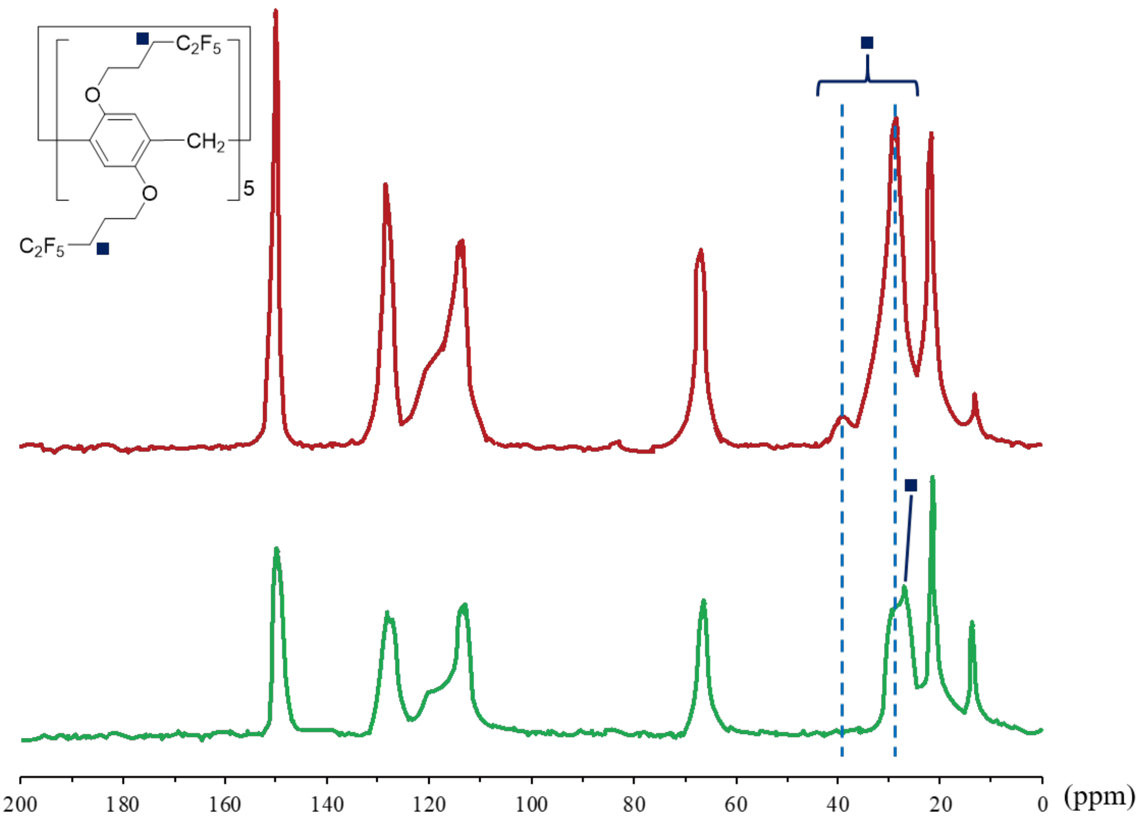


**Fig. S29** Solid-state $^{13}C$ NMR spectra of ***a*-F5** (upper side) and ***c*-(F5⊃H)** (lower side).

Obvious peak shifts of the signals from fluoroalkyl groups of **F5** (blue square) were observed before and after exposure to *n*-hexane vapor, indicating that the structure of the fluoroalkyl groups mainly changed along with the transition from ***a*-F5** to ***c*-(F5⊃H)**. In addition, the peaks shifted to higher magnetic fields, suggesting that the hydrogen atoms bound to the carbon atoms illustrated blue squares were shielded by accepting electrons from electronegative fluorine atoms of the fluoroalkyl groups. Single-crystal X-ray structural analysis of **F5⊃H** (**Fig. 2d**) suggested the formation of fluoroalkyl layers and the intermolecular C–H···F hydrogen bonds in the ***c*-(F5⊃H)** structure. These results supported that the uptake of *n*-hexane guest vapor in the cavity of ***a*-F5** changed the structure of the fluoroalkyl groups and caused the intermolecular C–H···F hydrogen bonds, resulting in the formation of fluoroalkyl layers in ***c*-(F5⊃H)**.

## 6. Molecular electrostatic potential maps

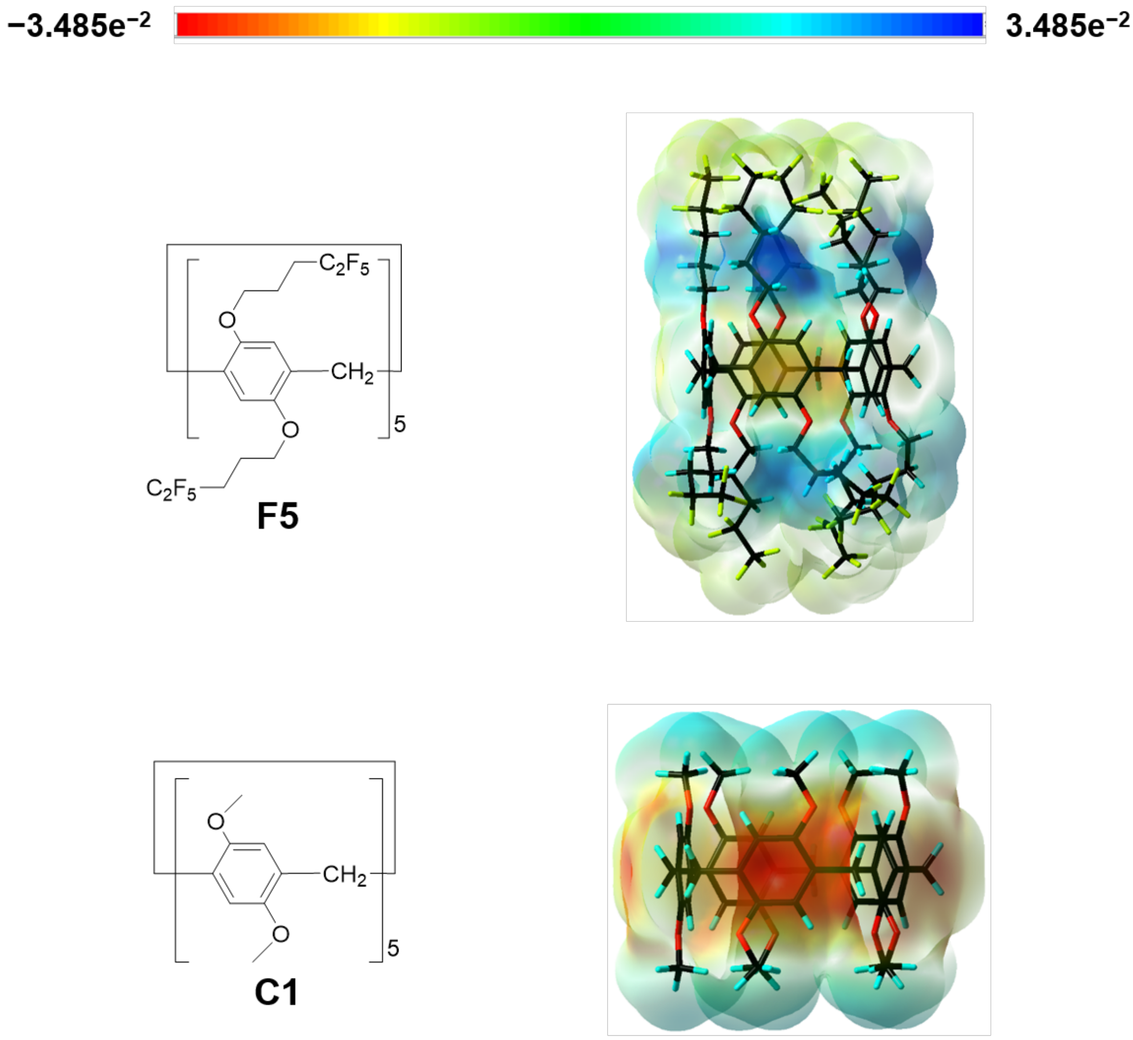


**Fig. S30** Molecular electrostatic potential maps of **F5** (upper side) and permethylated pillar[5]arene (**C1**) (lower side). F, O, C and H atoms are represented by yellow, red, black and light blue capped sticks, respectively.

## 7. State and contact angle changes by guest vapors

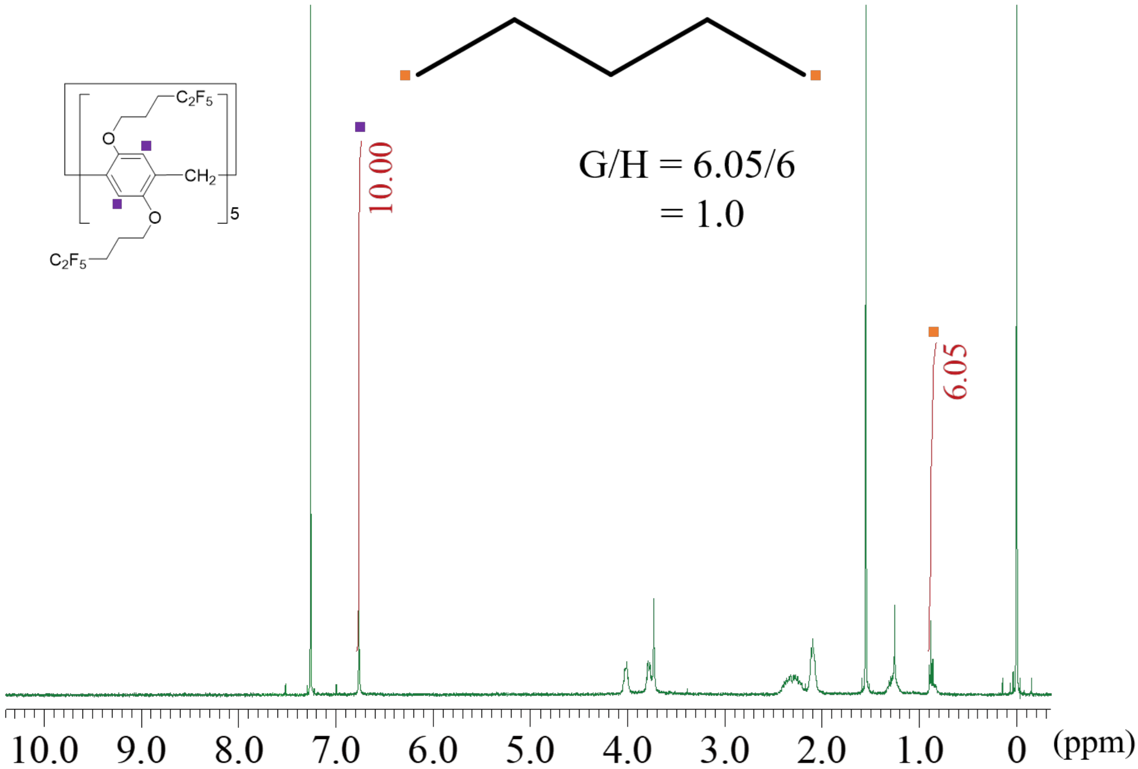


**Fig. S31** [1]H NMR spectrum of ***c*-(F5⊃P)** ($CDCl_3$, 25 °C). The uptake ratio of *n*-pentane to **F5** (G/H) calculated from the integration ratio was 1.0.

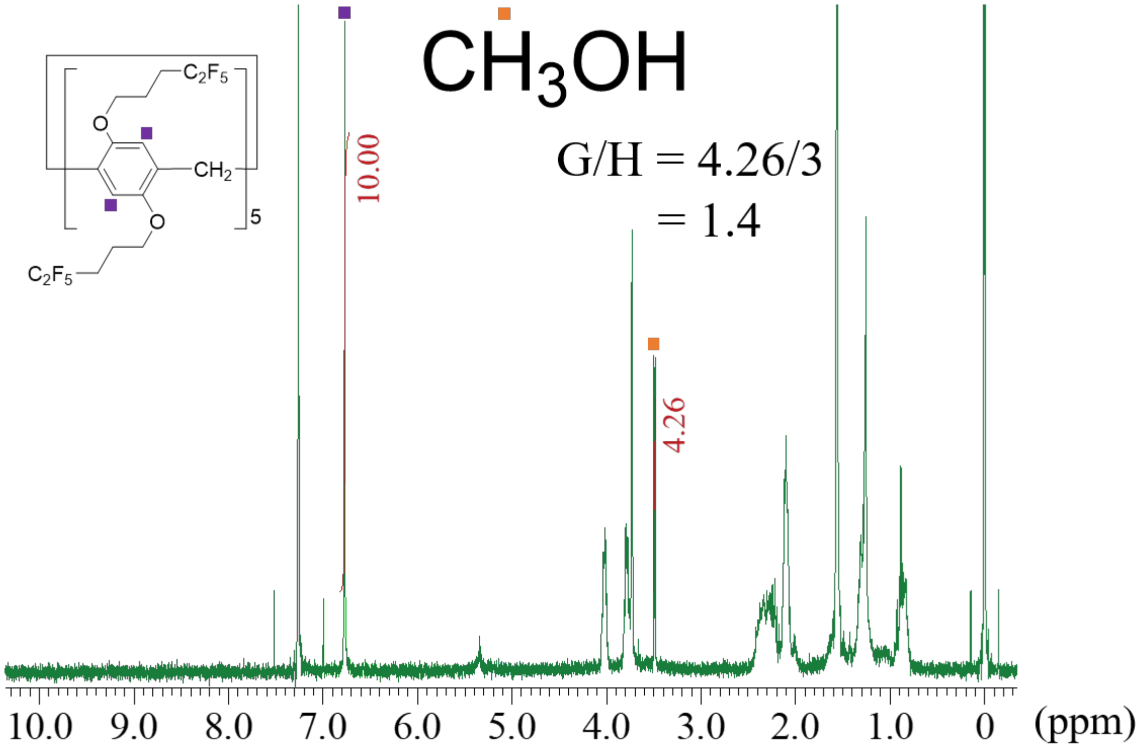


**Fig. S32** $^1$H NMR spectrum of ***c*-(F5⊃Methanol)** ($CDCl_3$, 25 °C). The uptake ratio of methanol to **F5** (G/H) calculated from the integration ratio was 1.4.

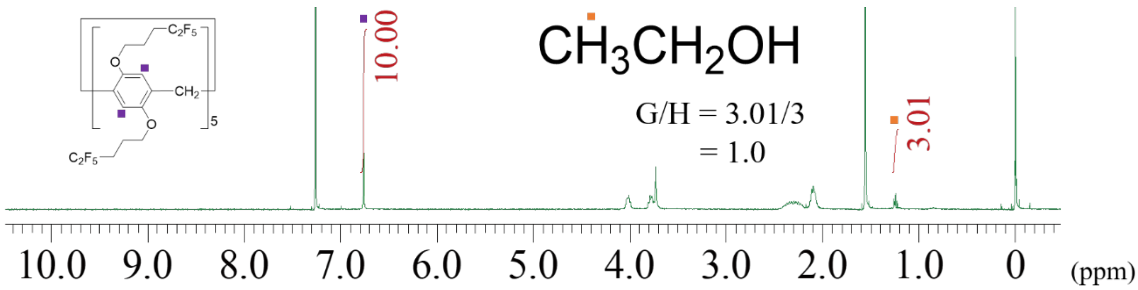


**Fig. S33** [1]H NMR spectrum of ***c*-(F5⊃Ethanol)** ($CDCl_3$, 25 °C). The uptake ratio of ethanol to **F5** (G/H) calculated from the integration ratio was 1.0.

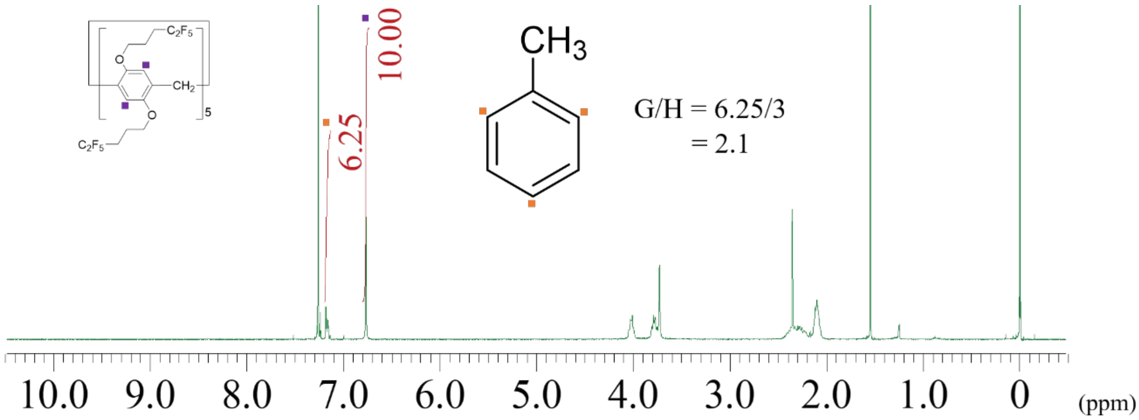


**Fig. S34** $^1$H NMR spectrum of ***c*-(F5⊃Toluene)** ($CDCl_3$, 25 °C). The uptake ratio of toluene to **F5** (G/H) calculated from the integration ratio was 2.1.

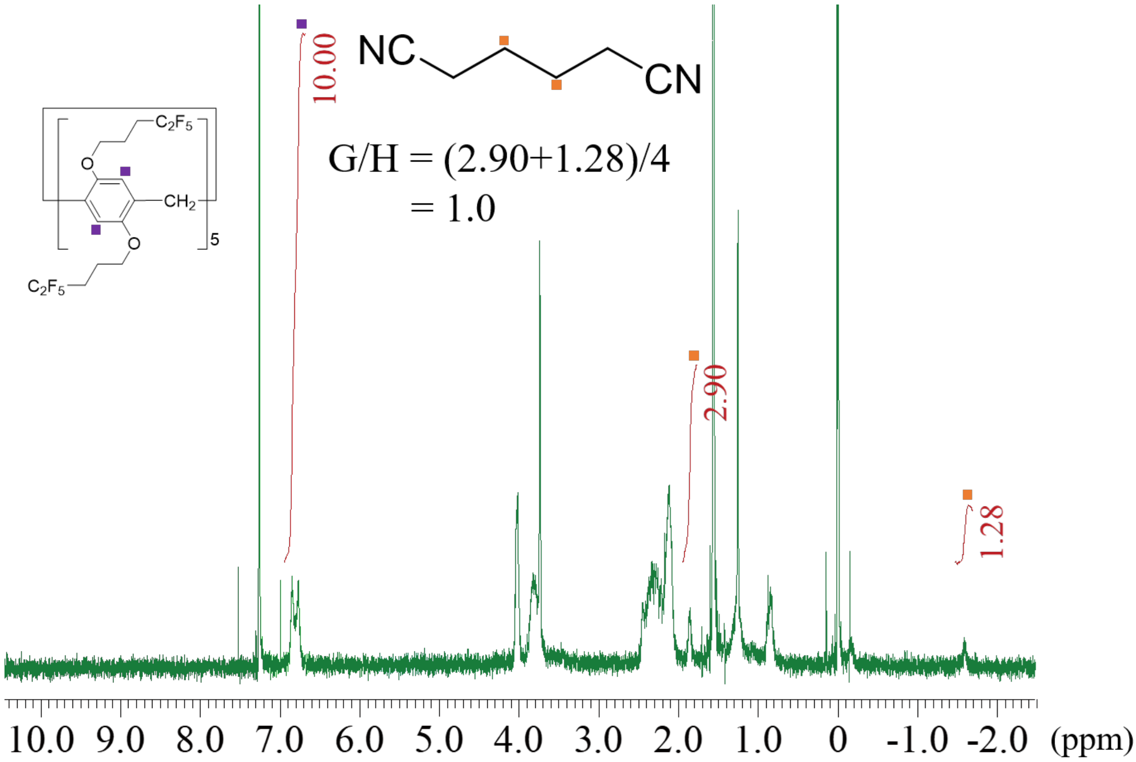


**Fig. S35** [1]H NMR spectrum of ***c*-(F5⊃1,4-Dicyanobutane)** ($CDCl_3$, 25 °C). The uptake ratio of 1,4-dicyanobutane to **F5** (G/H) calculated from the integration ratio was 1.0.

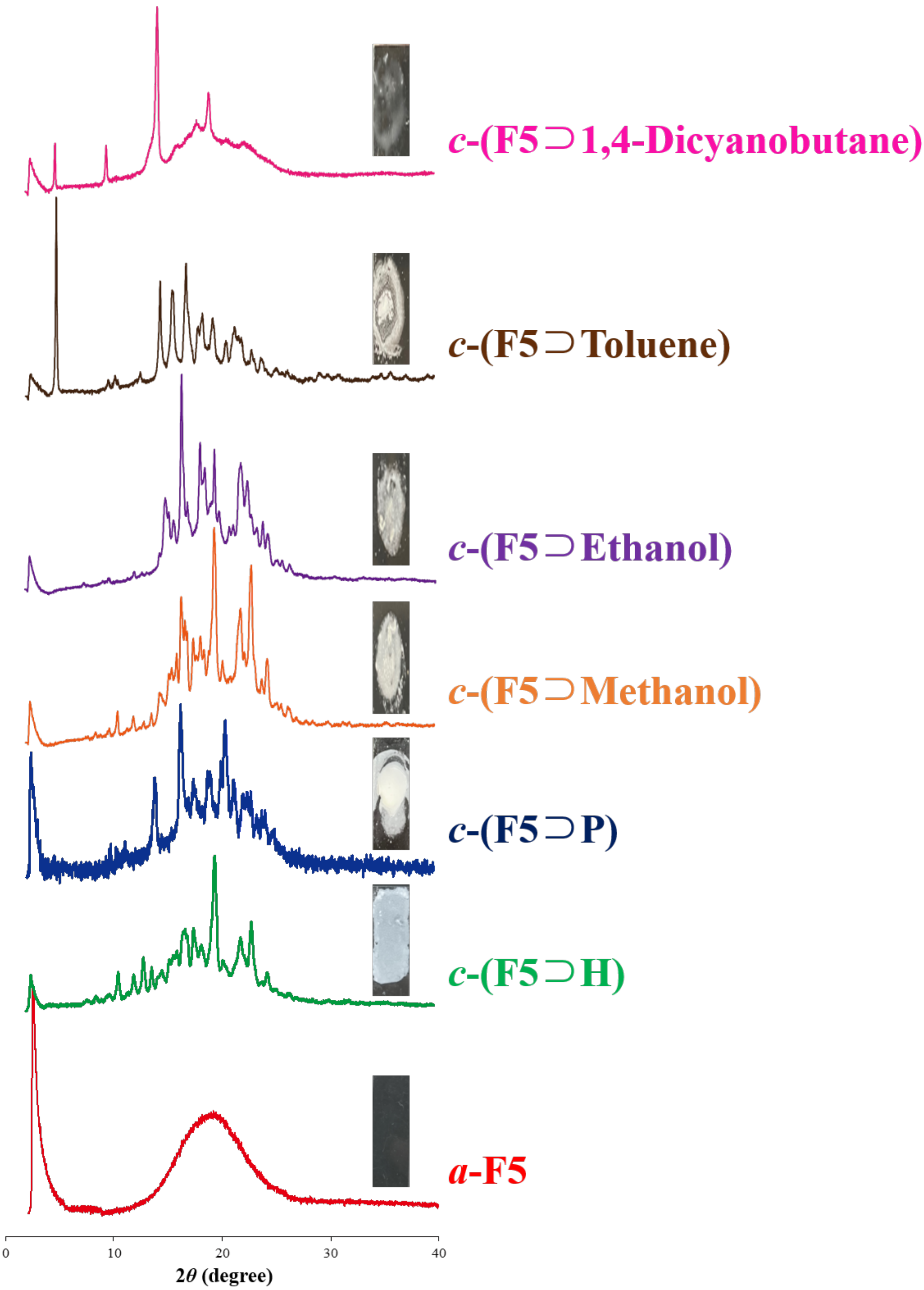


**Fig. S36** PXRD patterns of ***a*-F5** (red), ***c*-(F5⊃H)** (green), ***c*-(F5⊃P)** (blue), ***c*-(F5⊃Methanol)** (orange), ***c*-(F5⊃Ethanol)** (violet), ***c*-(F5⊃Toluene)** (brown) and ***c*-(F5⊃1,4-Dicyanobutane)** (pink).

**Table S2** Water contact angles of the complexes of **F5** with its guest vapors. One standard error is calculated from five independent measurements.

| Guest Vapor | Water Contact Angle (°) |
|---|---|
| No Guest | 98±3 |
| *n*-Hexane | 112±1 |
| *n*-Pentane | 119±2 |
| Methanol | 101±5 |
| Ethanol | 98±4 |
| Toluene | 101±2 |
| 1,4-Dicyanobutane | 101±0 |

The noticeable increases in the water contact angles of **F5** were observed only in ***c*-(F5⊃H)** and ***c*-(F5⊃P)**.

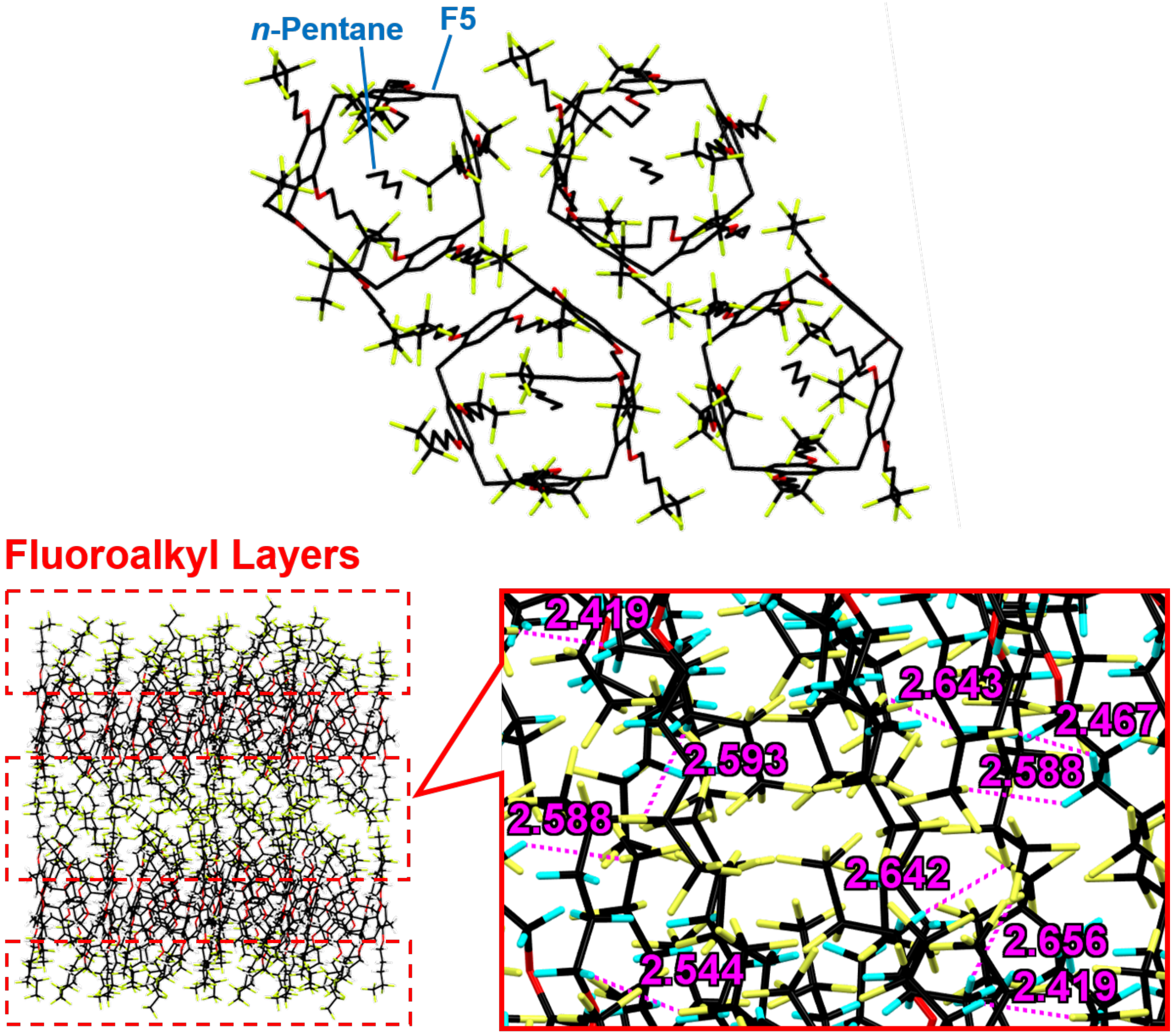


**Fig. S37** Single-crystal structures of **F5⊃P**; all labeled distances of intermolecular C–H···F hydrogen bonds are given in angstrom orders. F, O, C and H atoms are represented by yellow, red, black and light blue capped sticks, respectively.

**F5** formed 1:1 host–guest complex with *n*-pentane, corresponding to aforementioned $^{1}$H NMR study of ***c*-(F5⊃P)** (**Fig. S31**). The complex formed a high-symmetrical and pillar-shaped structure, resulting in the formation of channel structures. Fluoroalkyl layer formation was induced by intermolecular C–H···F hydrogen bonds.

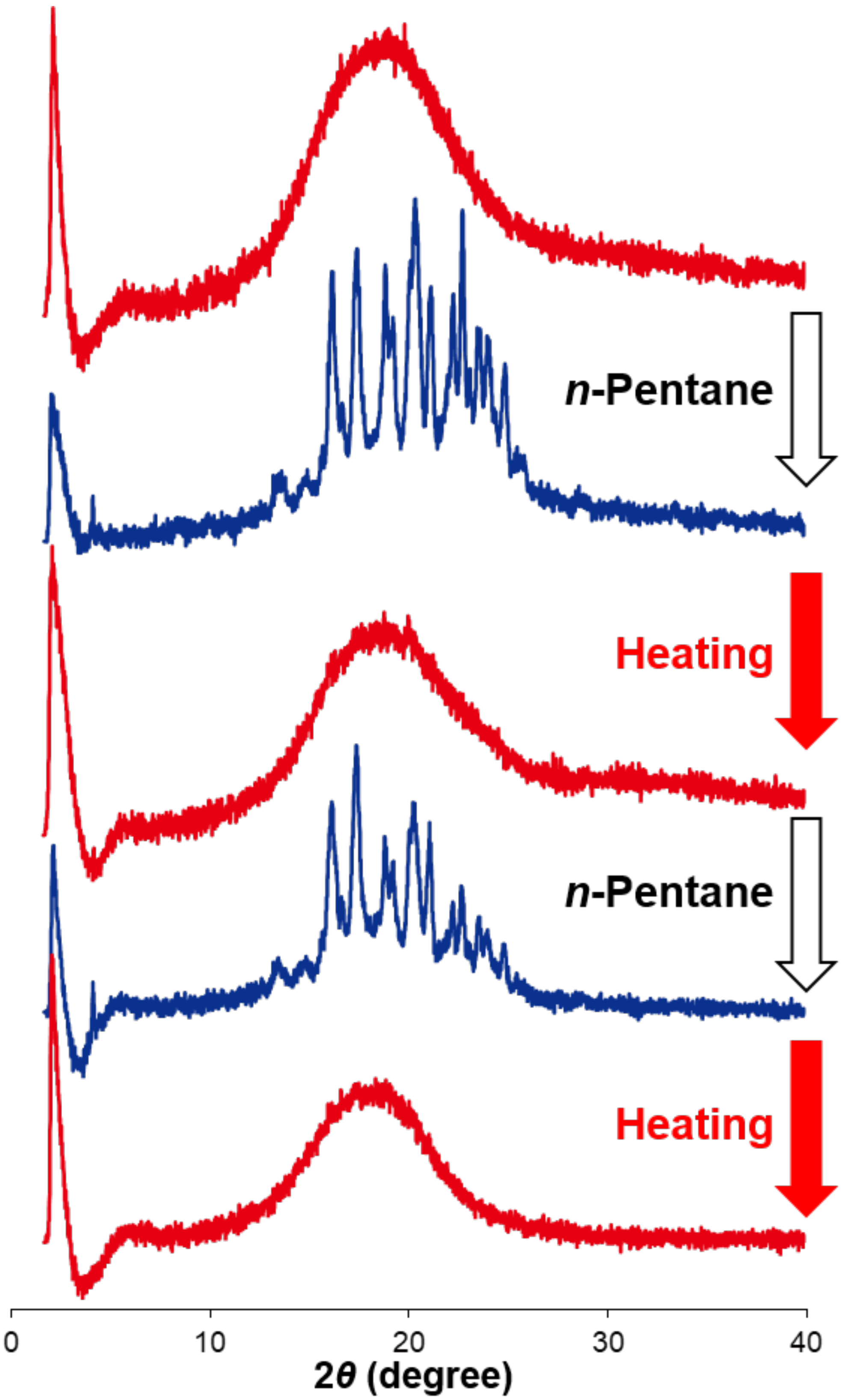


**Fig. S38** PXRD patterns of **F5** by exposing ***a*-F5** to *n*-pentane vapor and heating ***c*-(F5⊃P)** at 160 °C.

**Table S3** Contact angles of 1-bromonaphthalene on the surfaces of ***a*-F5**, ***c*-(F5⊃H)** and ***c*-(F5⊃P)**. One standard error is calculated from five independent measurements.

| Compound | Contact Angle of 1-Bromonaphthalene (°) |
|---|---|
| ***a*-F5** | 40±1 |
| ***c*-(F5⊃H)** | 40±2 |
| ***c*-(F5⊃P)** | 29±3 |

***c*-(F5⊃P)** showed smaller contact angle of 1-bromonaphthalene than ***a*-F5** and ***c*-(F5⊃H)**, suggesting that the rougher surface of ***c*-(F5⊃P)** affected the decrease in oil repellency.

**Table S4** Water contact angles of reference compounds before or after exposure to *n*-hexane or *n*-pentane vapors. One standard error is calculated from five independent measurements.

| Compound | Guest Vapor | Water Contact Angle (°) |
|---|---|---|
| **F3** | No Guest | 98±1 |
| **F3** | *n*-Hexane | 80±3 |
| **F3** | *n*-Pentane | 85±4 |
| **C5** | No Guest | 98±1 |
| **C5** | *n*-Hexane | 106±1 |
| **C5** | *n*-Pentane | 102±1 |
| **F13**[a] | *n*-Hexane | 84±4 |
| **Monomer Unit**[b] | No Guest | 74±1 |

[a] *n*-Hexane could not be removed from **F13**.

[b] **Monomer Unit** with no macrocyclic structure did not take up the guest vapors.

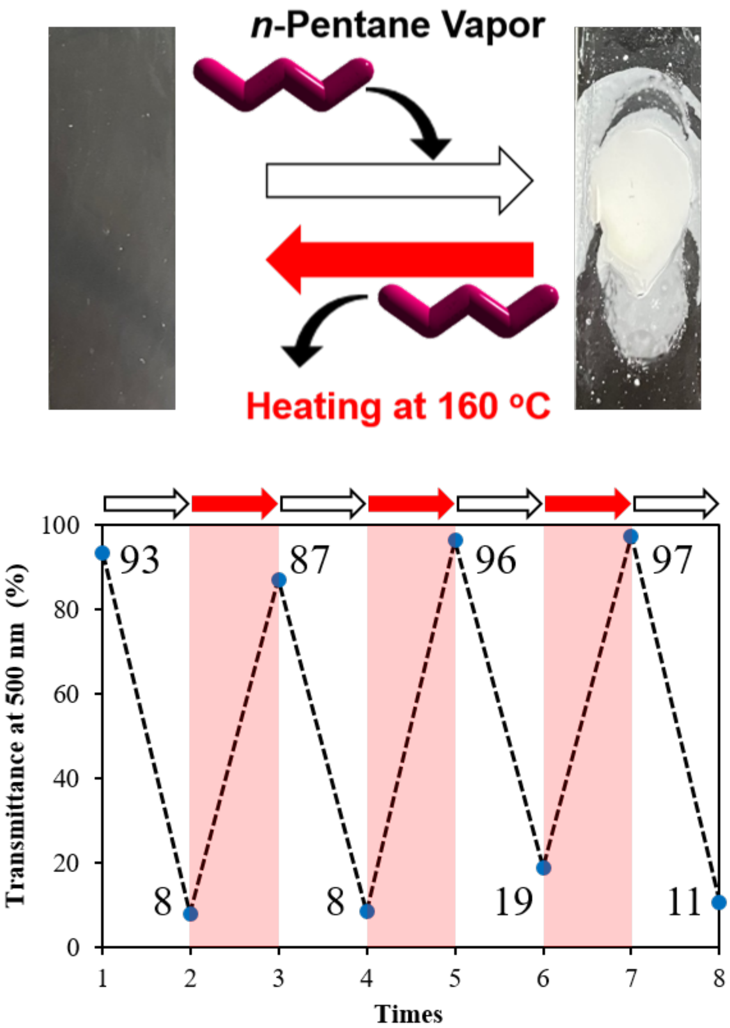


**Fig. S39** Photographs (upper side) and transmittance changes at 500 nm (lower side) of **F5** by exposing ***a*-F5** to *n*-pentane vapor (odd times) and heating ***c*-(F5⊃P)** at 160 °C (even times).

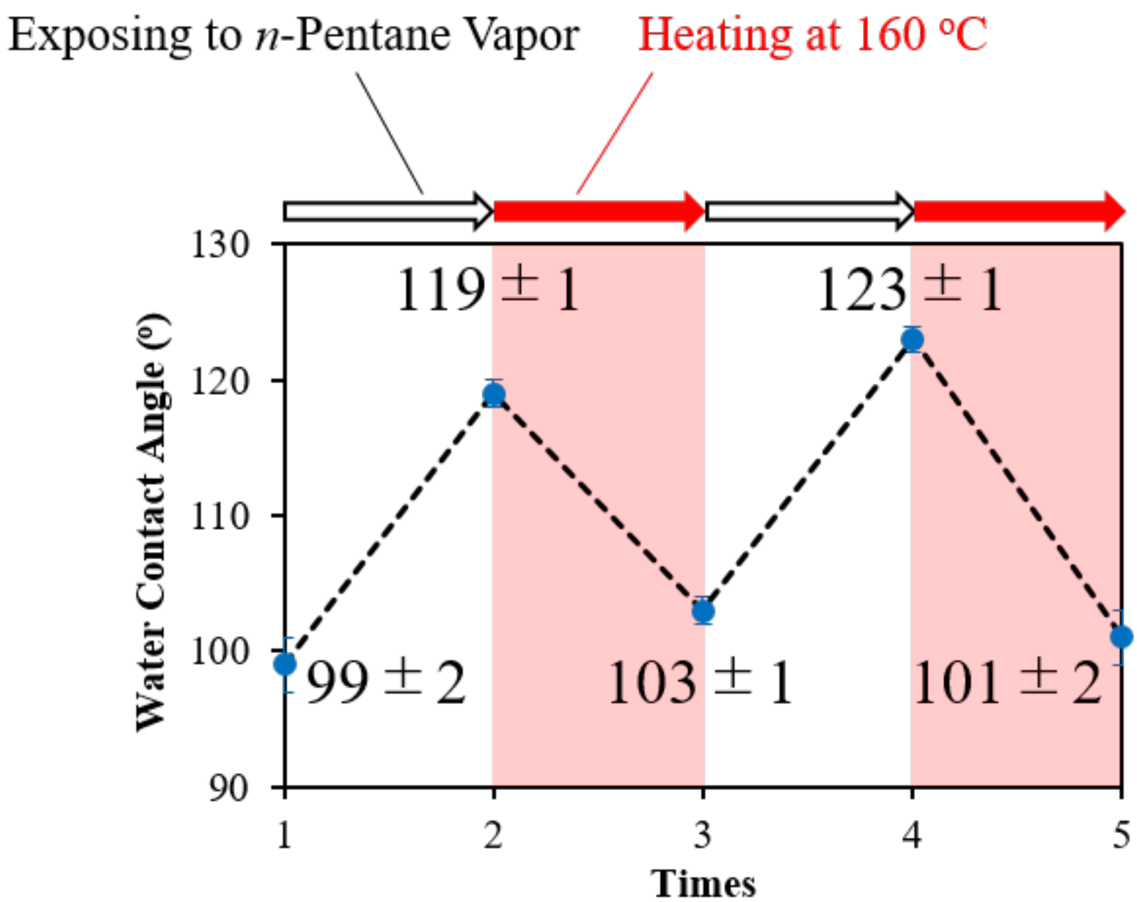


**Fig. S40** Water contact angle changes of **F5** by exposing ***a*-F5** to *n*-pentane vapor (odd times) and heating ***c*-(F5⊃P)** at 160 °C (even times). The error bars represent one standard error from five independent measurements.

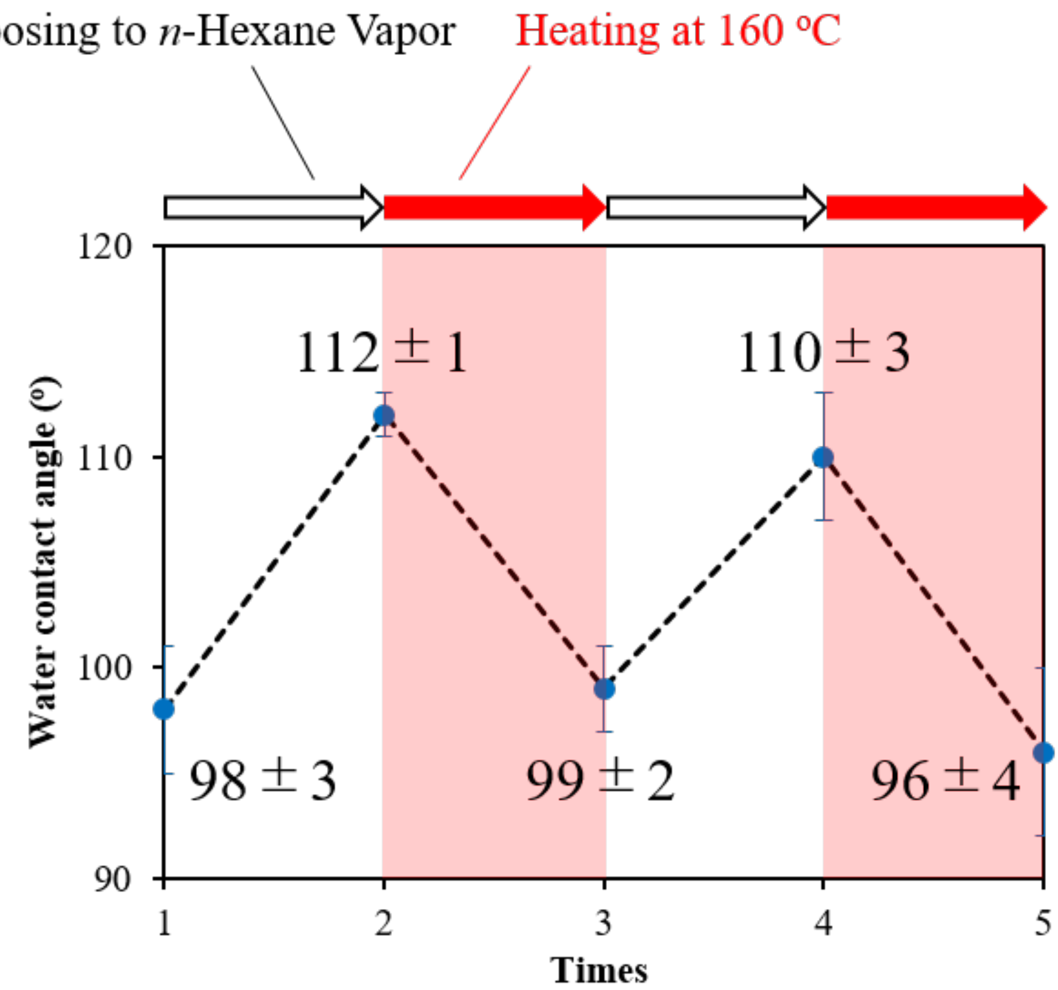


**Fig. S41** Water contact angle changes of **F5** by exposing ***a*-F5** to *n*-hexane vapor (odd times) and heating ***c*-(F5⊃H)** at 160 °C (even times). The error bars represent one standard error from five independent measurements.

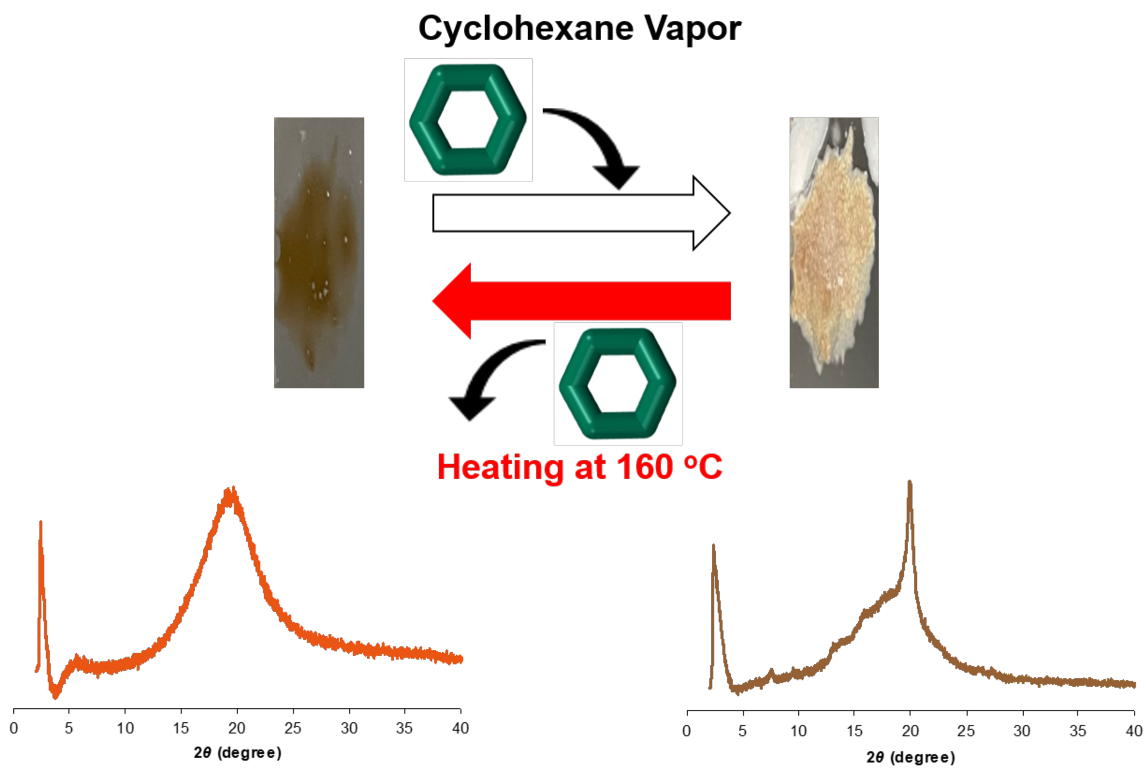


**Fig. S42** Photographs and PXRD patterns of **[6]F5** before (left) and after (right) exposure to cyclohexane vapor.

From PXRD measurements, the resulting sample after exposure to cyclohexane vapor showed sharp diffraction peaks in contrast to no sharp diffraction peaks of the amorphous sample before exposure to cyclohexane vapor, indicating the amorphous to crystalline phase change as **F5** did. From this result, $C_2F_5$ groups are good substituents to produce the guest vapor-responsive molecular glasses.

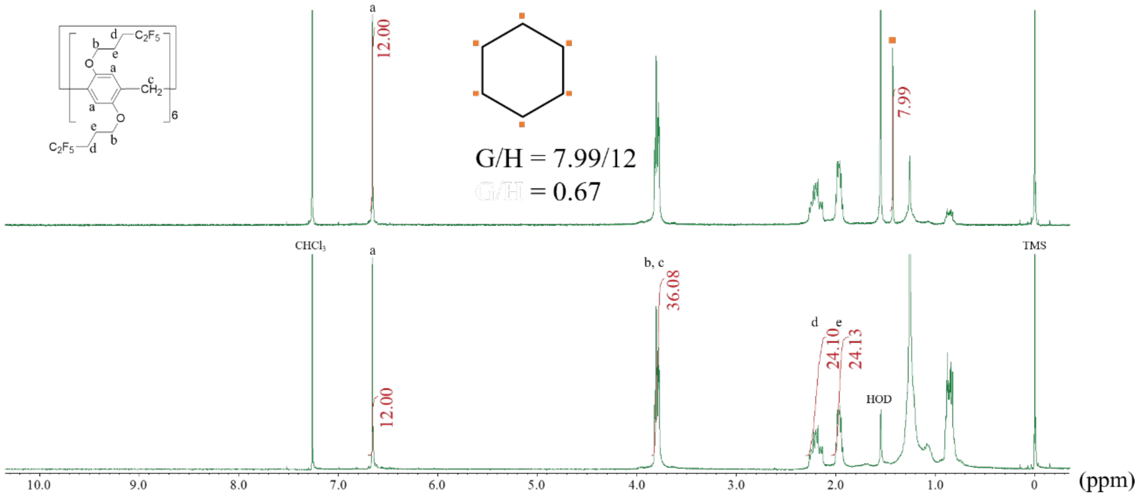


**Fig. S43** $^{1}$H NMR spectra of **[6]F5** ($CDCl_3$, 25 °C) before (lower side) and after (upper side) exposure to cyclohexane vapor. The uptake ratio of cyclohexane to **[6]F5** (G/H) calculated from the integration ratio was 0.67.

## 8. Time-dependent changes by exposing ***a*-F5** to ***n*-pentane vapor**

**Table S5** Time-dependent changes in uptake ratios of *n*-pentane to ***a*-F5**.

| Time (min) | Uptake Ratio |
|---|---|
| 0 | 0.011 |
| 3 | 0.34 |
| 5 | 0.51 |
| 10 | 0.52 |
| 15 | 0.63 |
| 25 | 0.75 |
| 30 | 0.78 |
| 45 | 0.95 |
| 60 | 1.0 |
| 120 | 1.1 |

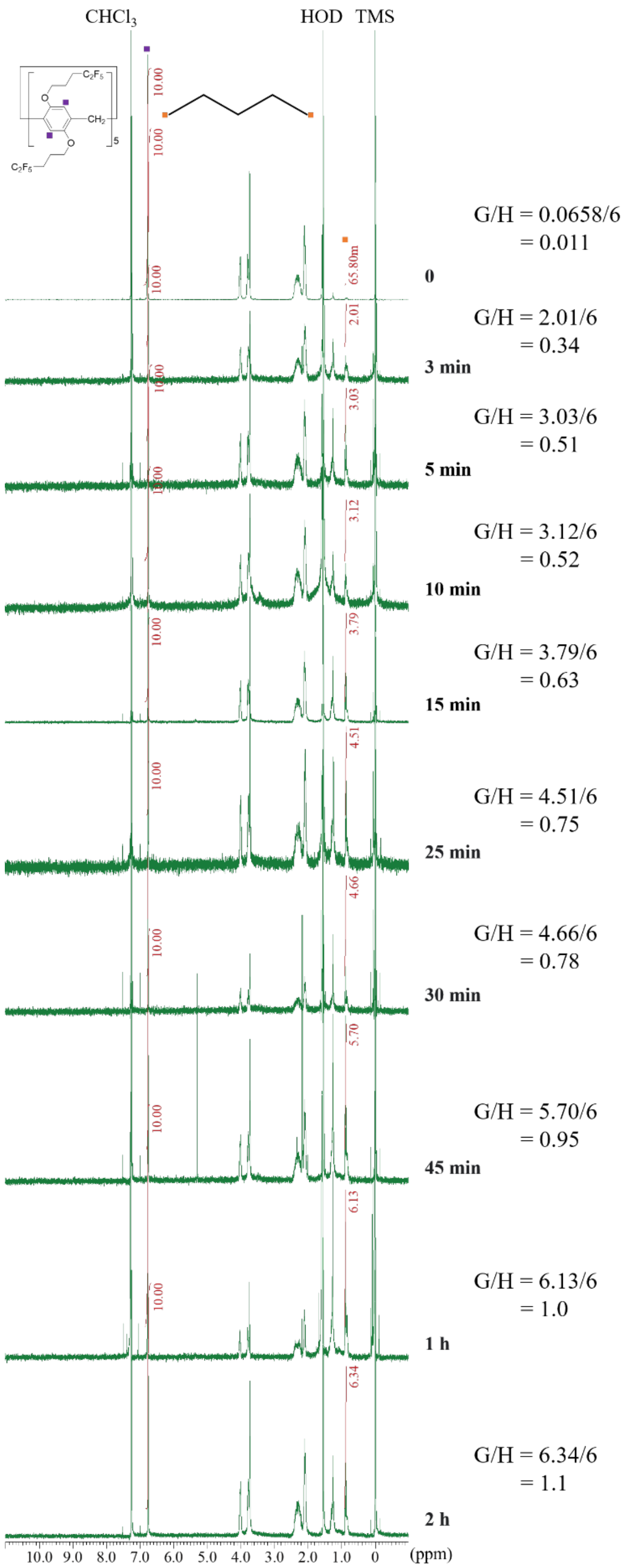


**Fig. S44** $^1$H NMR spectra of time-dependent changes in uptake ratios of *n*-pentane to ***a*-F5** ($CDCl_3$, 25 °C). The ratios are denoted as G/H.

**Table S6** Time-dependent changes in water contact angles of **F5** by exposing ***a*-F5** to *n*-pentane vapor. One standard error is calculated from five independent measurements.

| Time (min) | Water Contact Angle (°) |
| --- | --- |
| 0 | 99±1 |
| 3 | 104±2 |
| 5 | 105±1 |
| 10 | 108±1 |
| 15 | 111±1 |
| 25 | 113±1 |
| 30 | 112±1 |
| 45 | 117±1 |
| 60 | 121±2 |
| 120 | 121±1 |

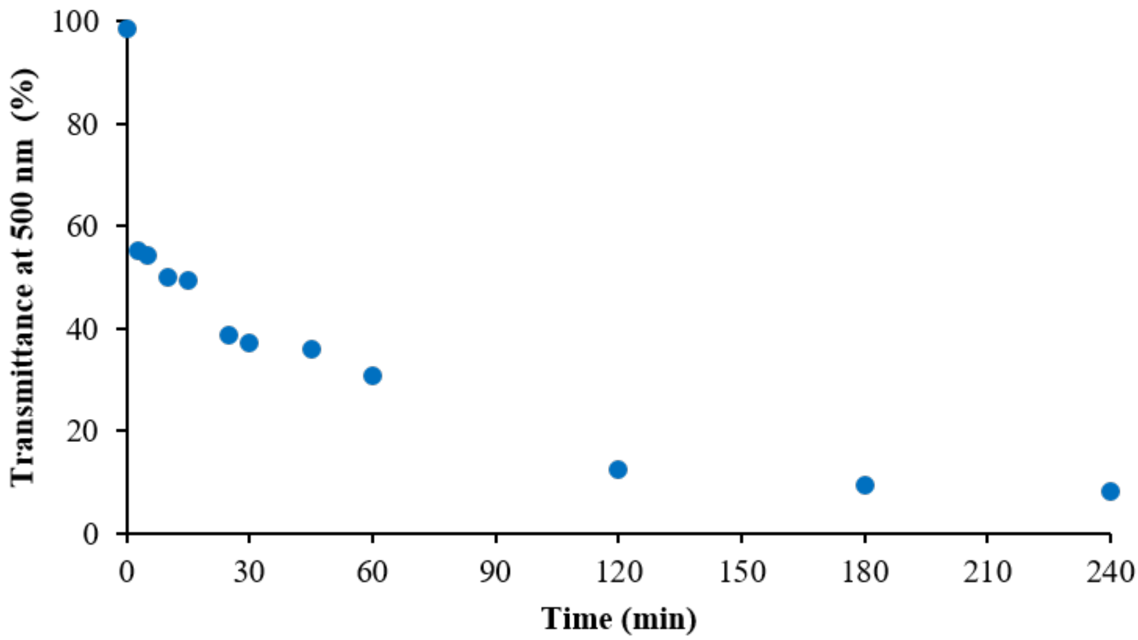


**Fig. S45** Time-dependent changes in transmittances at 500 nm of **F5** by exposing ***a*-F5** to *n*-pentane vapor.

**Table S7** Time-dependent changes in transmittances at 500 nm of **F5** by exposing ***a*-F5** to *n*-pentane vapor.

| Time (min) | Transmittance at 500 nm (%) |
|---|---|
| 0 | 99 |
| 3 | 55 |
| 5 | 54 |
| 10 | 50 |
| 15 | 49 |
| 25 | 39 |
| 30 | 37 |
| 45 | 36 |
| 60 | 31 |
| 120 | 13 |
| 180 | 9 |
| 240 | 8 |

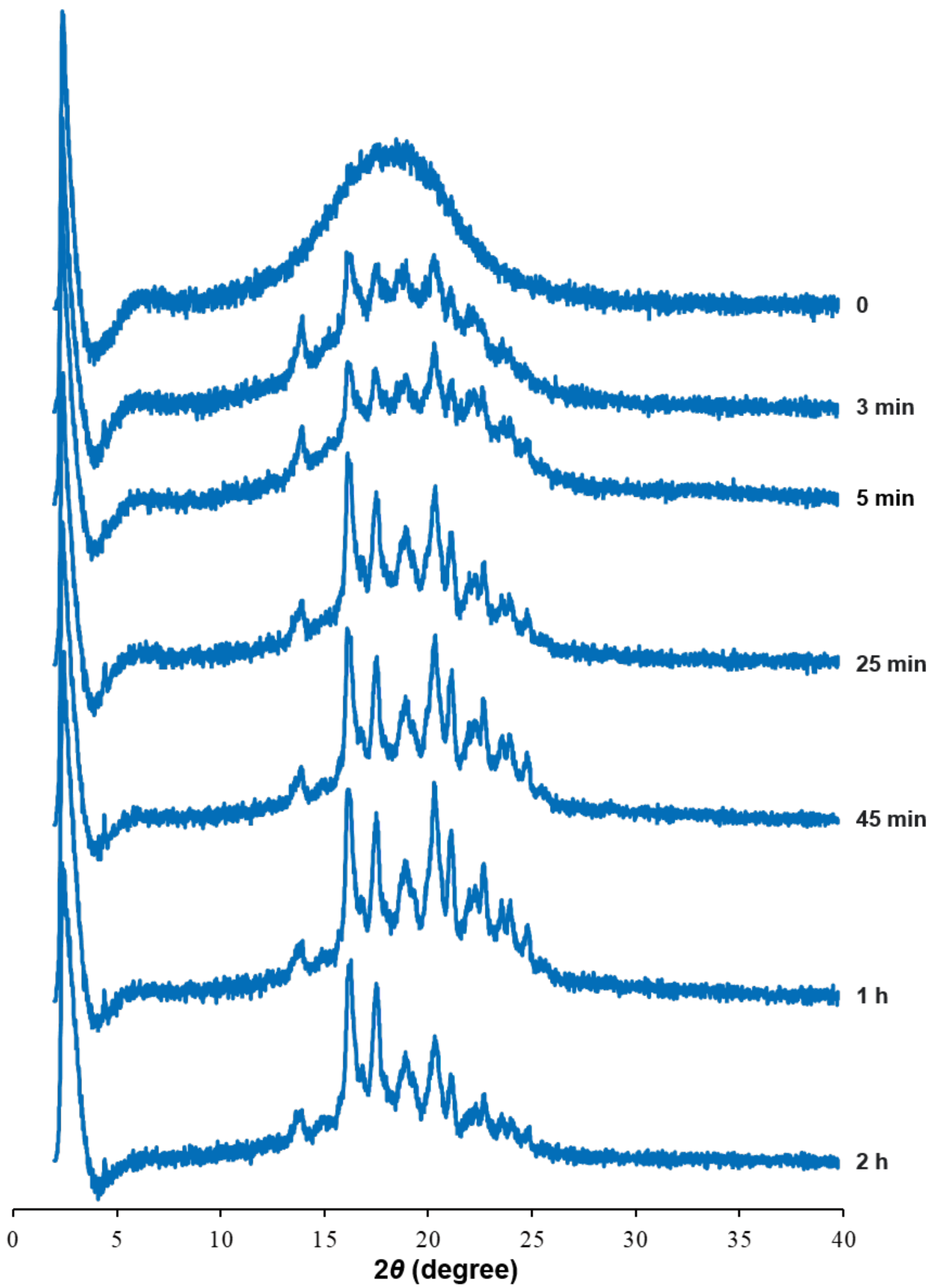

**Fig. S46** Time-dependent PXRD pattern changes of **F5** by exposing ***a*-F5** to *n*-pentane vapor.

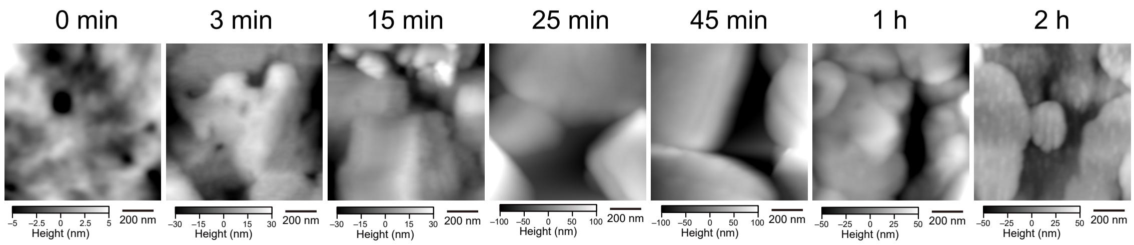


**Fig. S47** Time-dependent AFM image changes of **F5** by exposing ***a*-F5** to *n*-pentane vapor.

Before exposure to *n*-pentane (0 min), flat surface structures were observed. After 3 min exposure, curved edge structures were formed and crystalline structures with linear edges began to appear in 15 min. The formation of the crystalline structures proceeded gradually and had been completed at 1 h.

**9. Comparison between PXRD patterns of F5⊃P and *c*-(F5⊃P)**

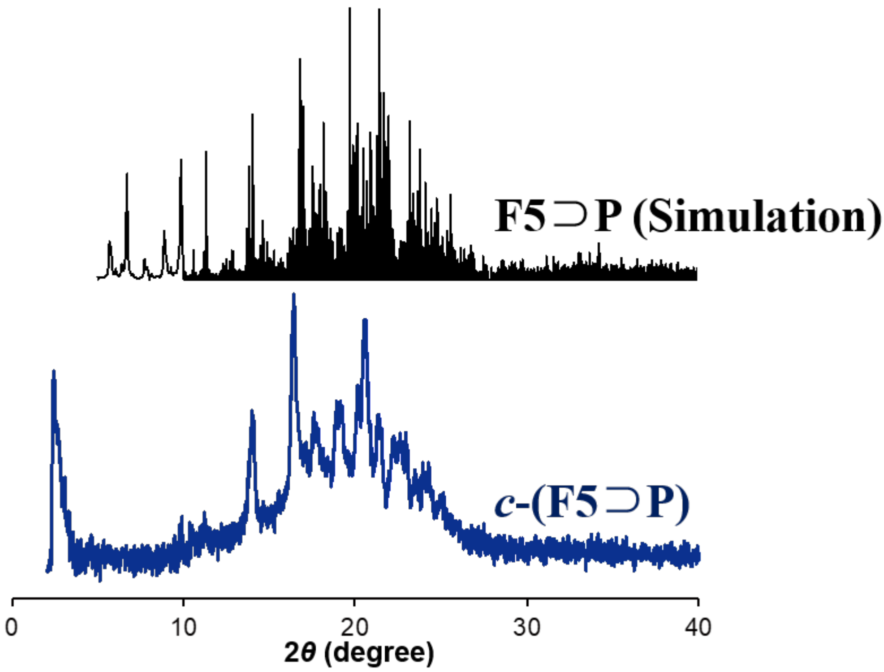


**Fig. S48** PXRD patterns of simulation from single crystal of **F5⊃P** (upper side) and ***c*-(F5⊃P)** (lower side).

The PXRD pattern simulated from a single crystal of **F5⊃P** was similar to that of ***c*-(F5⊃P)**, suggesting that uptake of *n*-pentane guest vapor in the **F5** cavity caused crystallization of amorphous state ***a*-F5**, whose structure was similar to that of the single crystal of **F5⊃P**. Therefore, the increase in water repellency of **F5** by uptake of *n*-pentane vapor was ascribed to the formation of fluoroalkyl layers.

## 10. Supplementary photographs

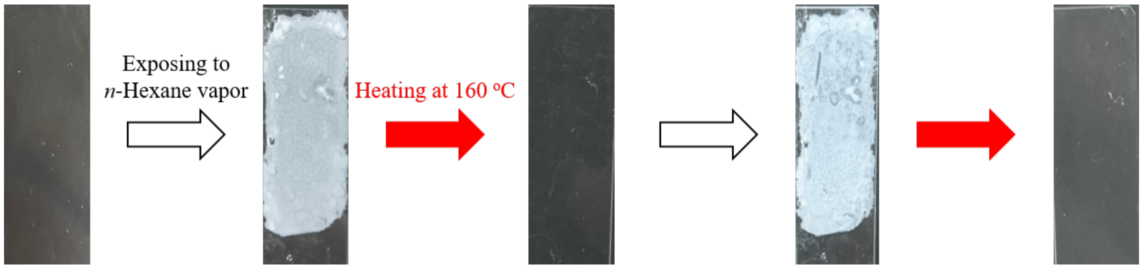


**Fig. S49** Photographs of **F5** by exposing ***a*-F5** to *n*-hexane vapor and heating ***c*-(F5⊃P)** at 160 °C repeatedly.

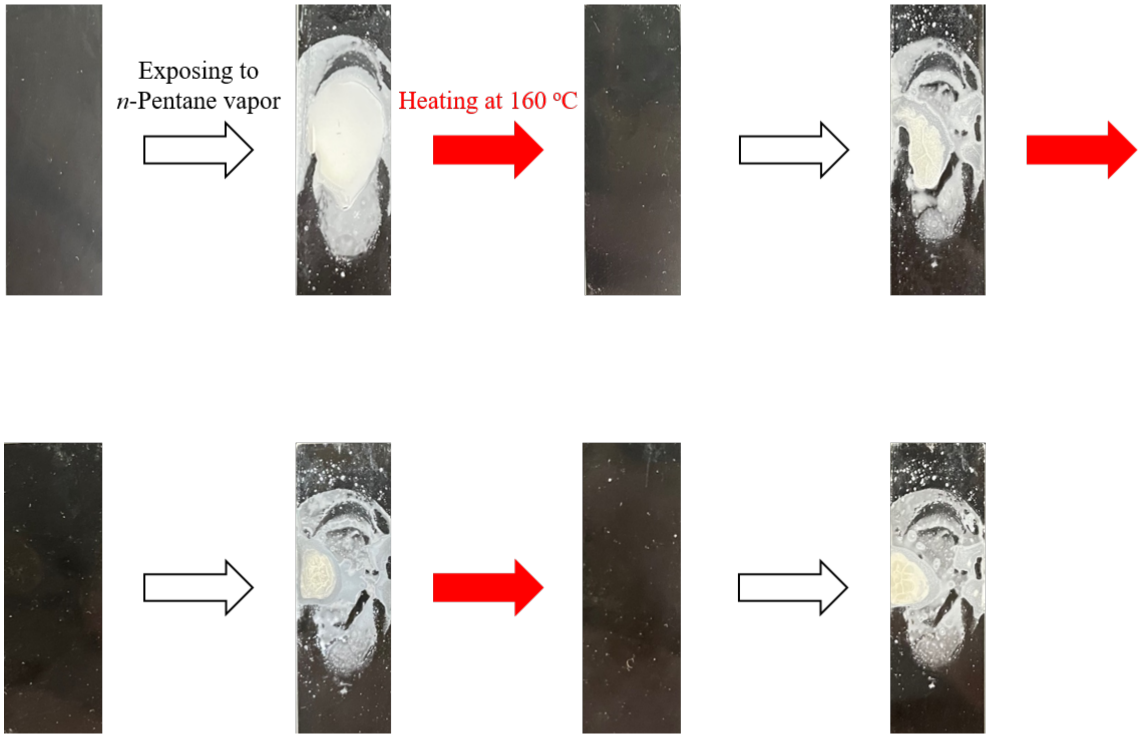


**Fig. S50** Photographs of **F5** by exposing ***a*-F5** to *n*-pentane vapor and heating ***c*-(F5⊃P)** at 160 °C repeatedly.

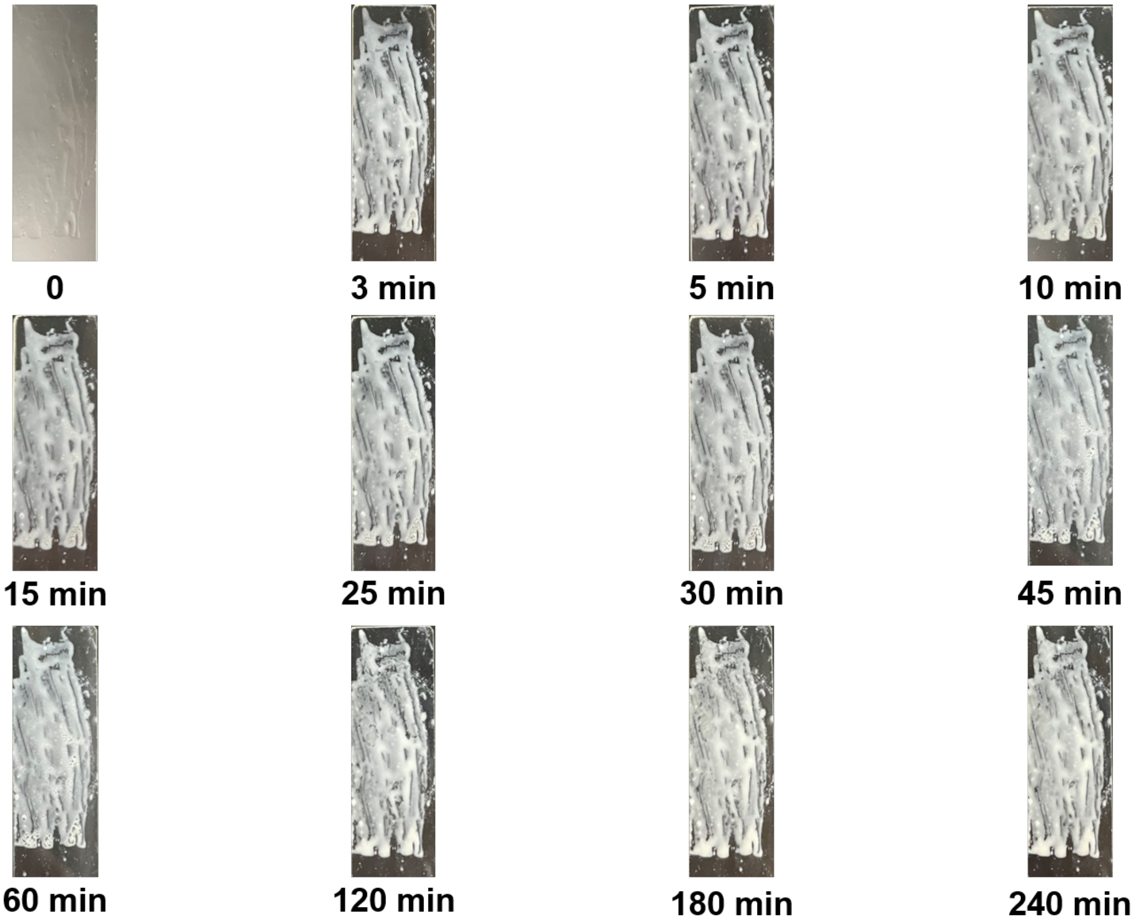

**Fig. S51** Photographs of time-dependent changes of **F5** by exposing ***a*-F5** to *n*-pentane vapor.

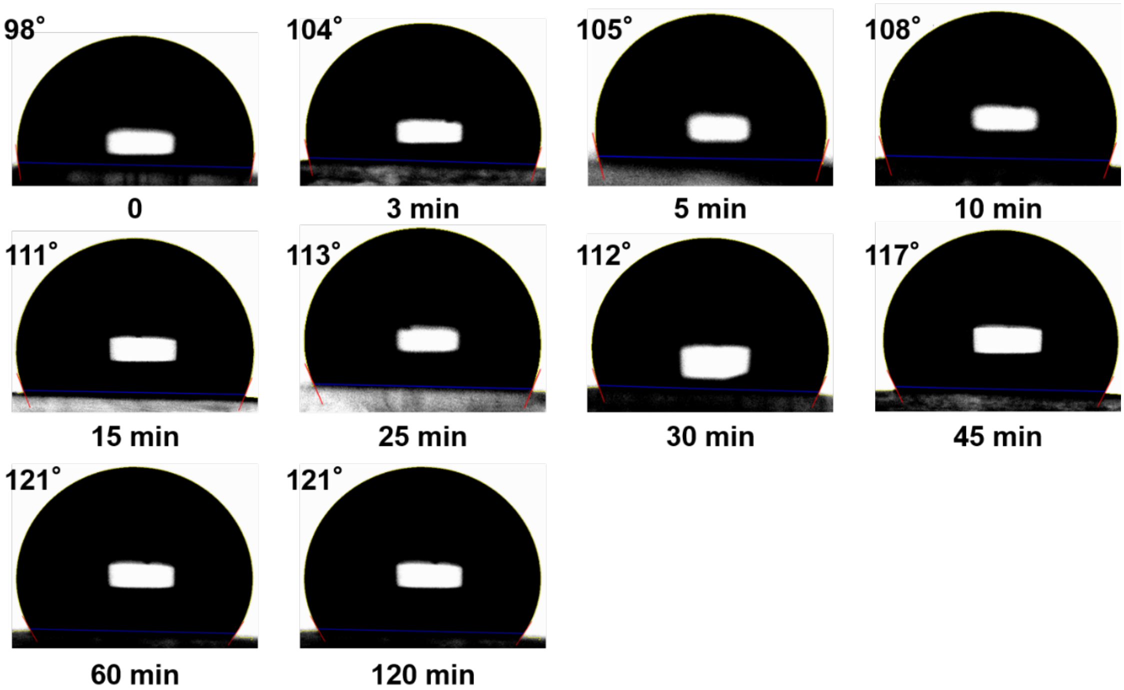


**Fig. S52** Photographs of time-dependent changes in water contact angles of **F5** by exposing ***a*-F5** to *n*-pentane vapor.

## 11. DSC curves of reference compounds

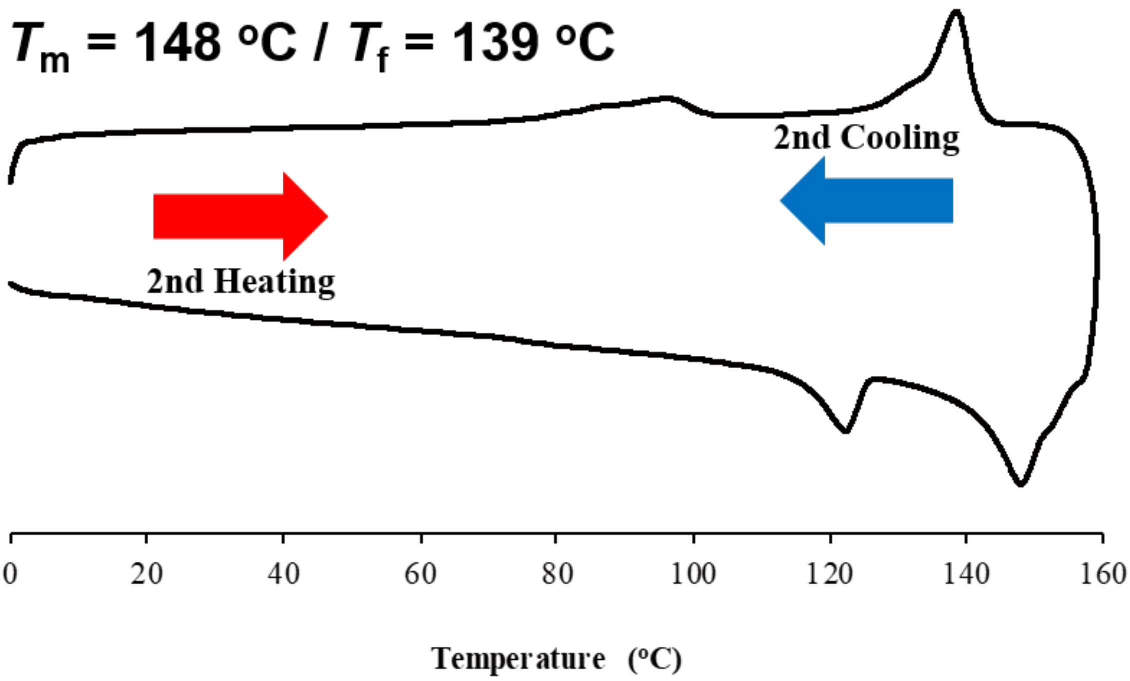


**Fig. S53** DSC second heating and cooling curve of **F3** (scanning rate: 10 °C/min).

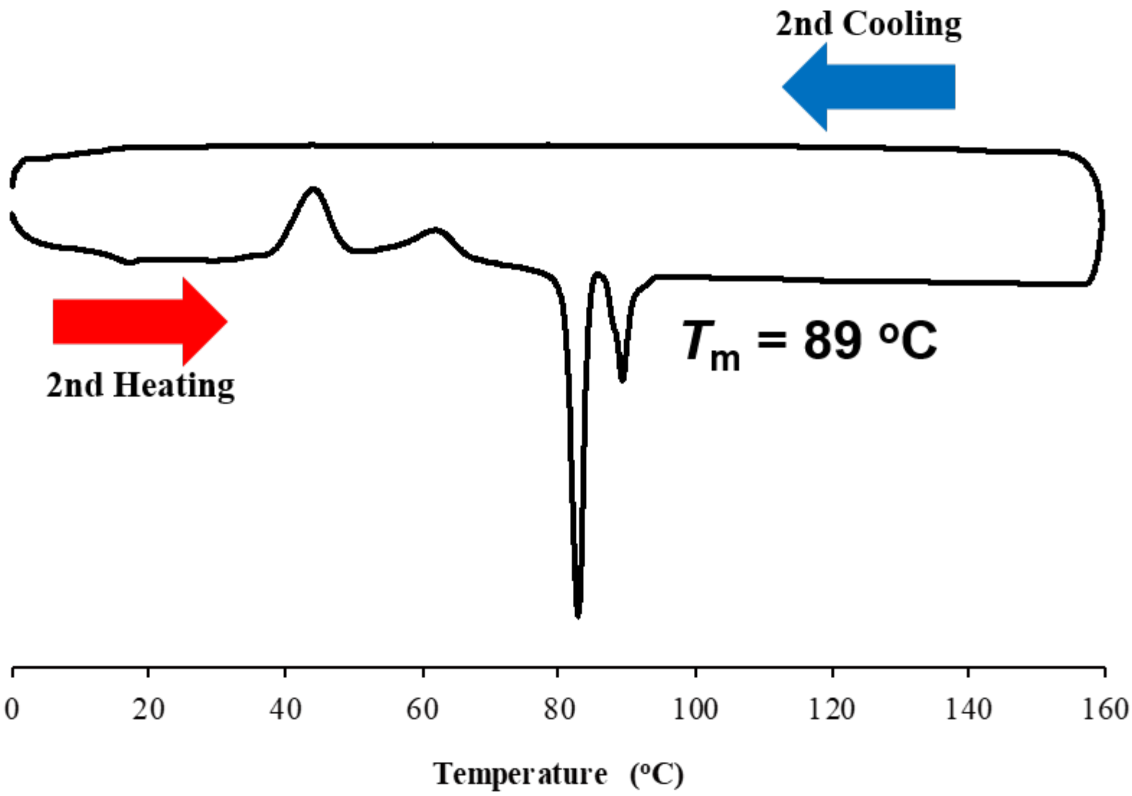


**Fig. S54** DSC second heating and cooling curve of **C5** (scanning rate: 10 °C/min).

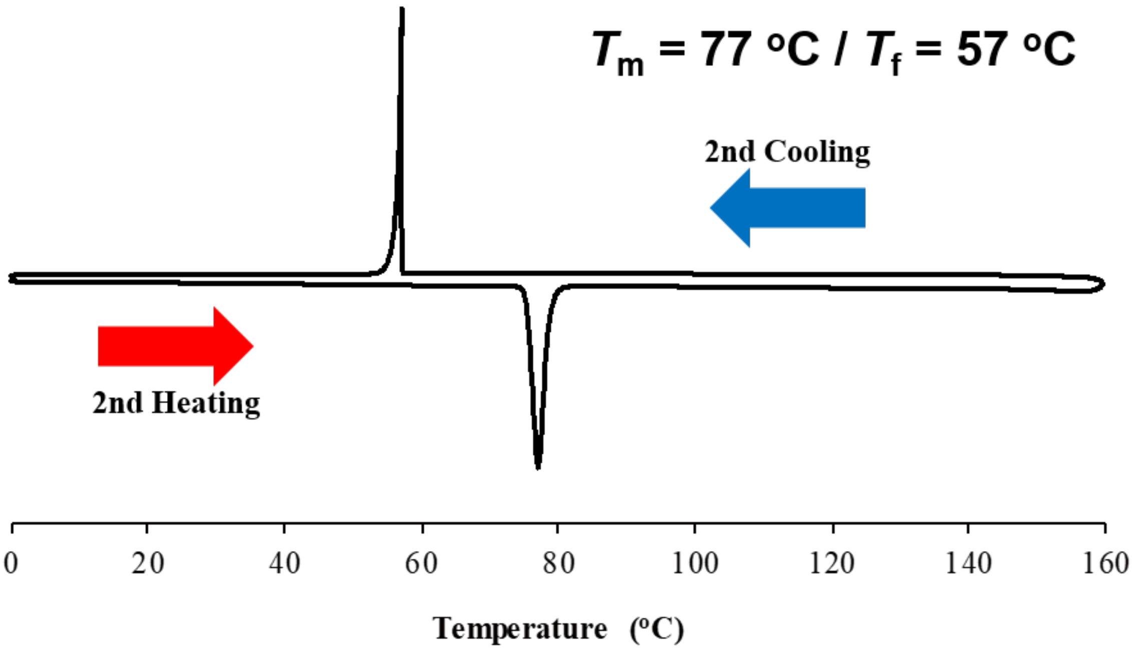

**Fig. S55** DSC second heating and cooling curve of **Monomer Unit** (scanning rate: 10 °C/min).

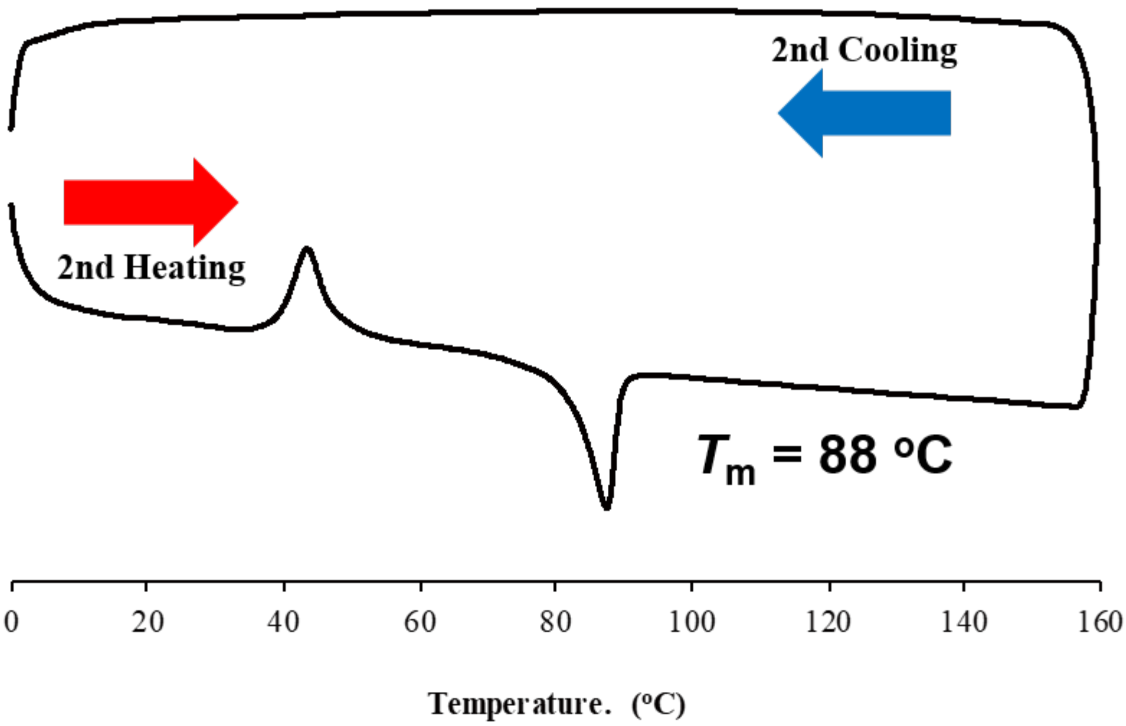


**Fig. S56** DSC second heating and cooling curve of **[6]F5** (scanning rate: 10 °C/min).

**12. Single-crystal structures**

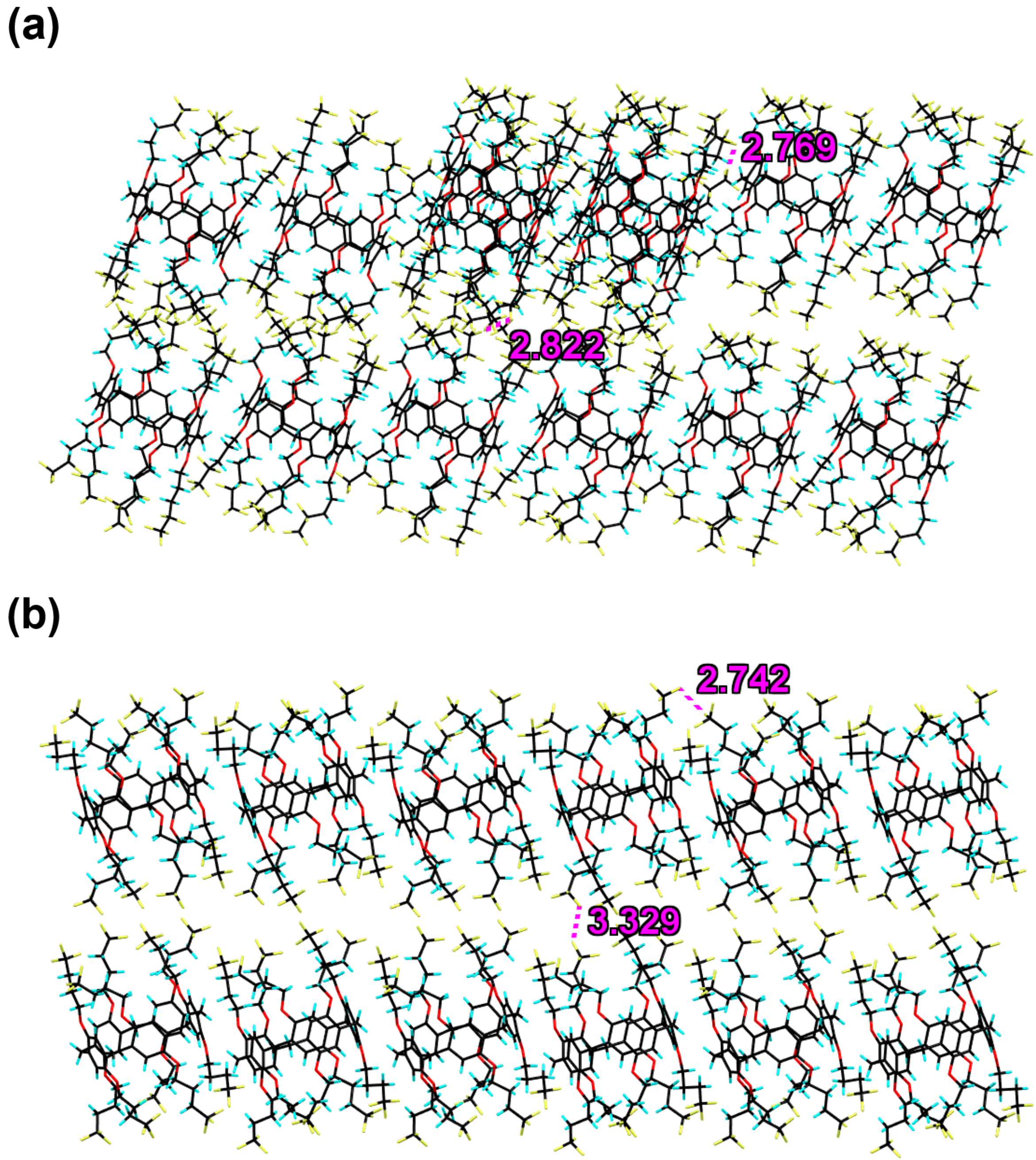

**(c)**

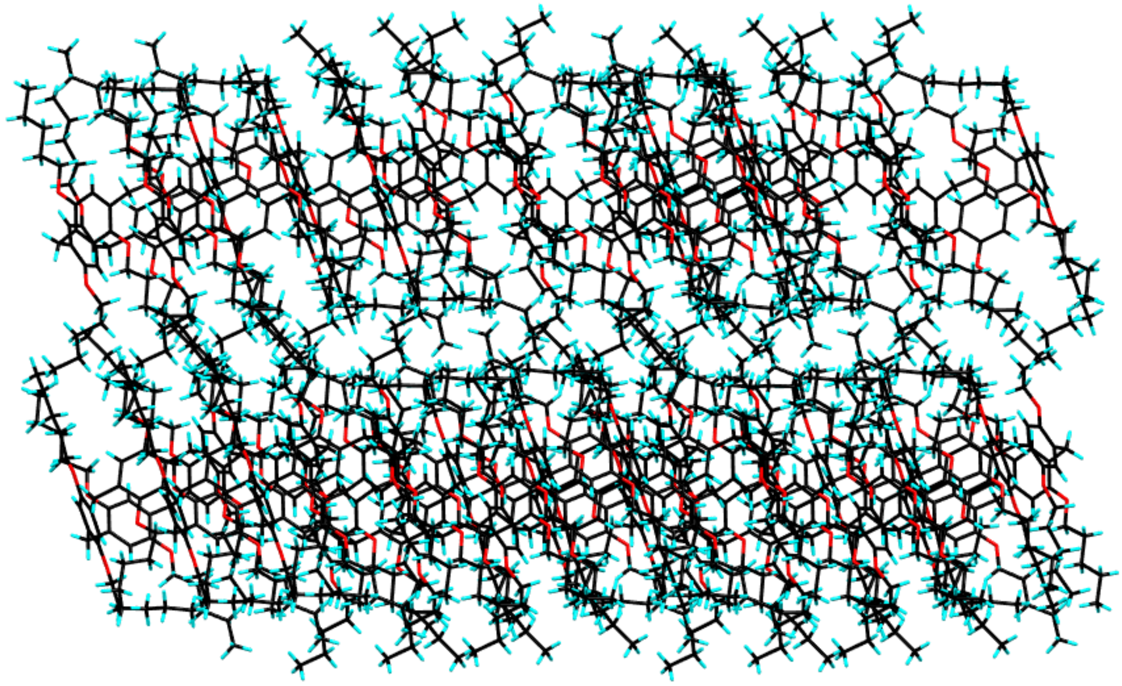

(d)

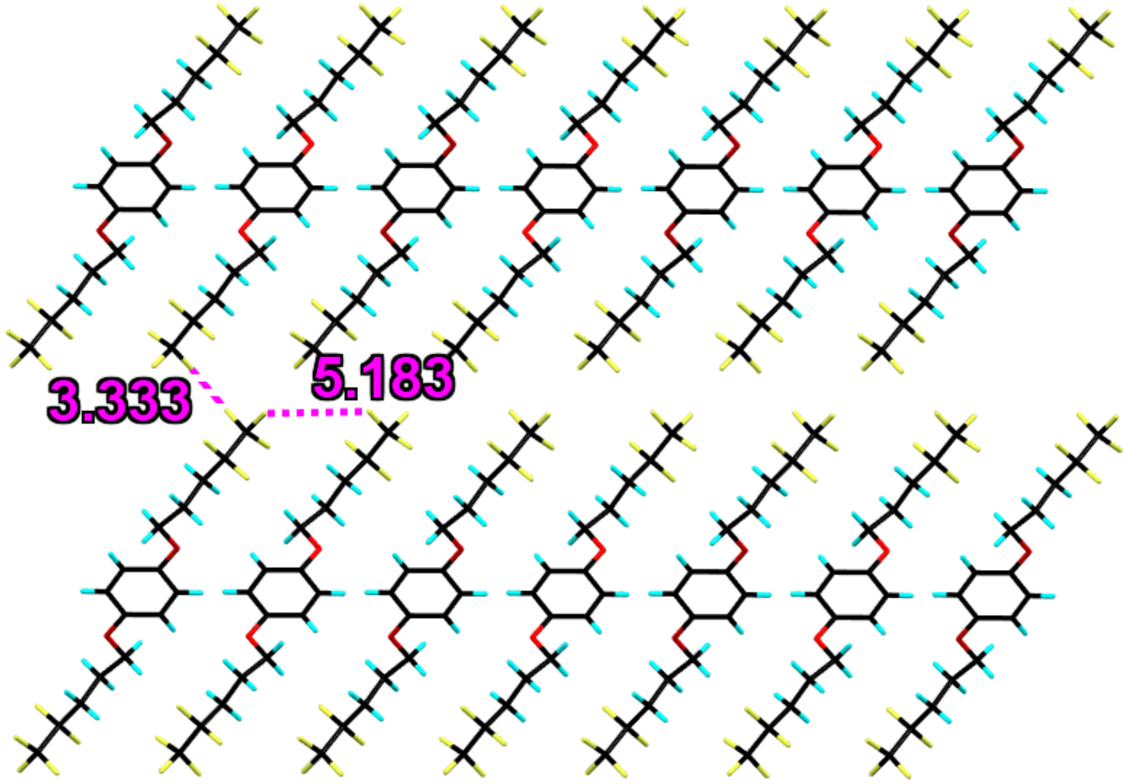


**Fig. S57** Single-crystal structures of (a) **F5⊃H**, (b) **F3⊃H**, (c) **C5⊃H** and (d) **Monomer Unit** (prepared from chloroform under *n*-hexane vapor); all labeled distances between intermolecular fluorine atoms are given in angstrom orders. F, O, C and H atoms are represented by yellow, red, black and light blue capped sticks, respectively. Guest molecules are omitted for clarity.

Compared to **F3⊃H** with short $CF_3$ groups (**Fig. S49b**), similar/closer distances between intermolecular fluorine atoms in same/adjacent layers are shown in **F5⊃H** (**Fig. S49a**), indicating that the number of fluorine atoms is important to show higher water repellency of ***c*-(F5⊃H)**. The distances in both same and adjacent layers in **F5⊃H** (**Fig. S49a**) are smaller than those of **Monomer Unit** with no macrocyclic structure (**Fig. S49d**). This suggests that fluorine atoms of **F5⊃H** with $C_2F_5$ groups aggregate more densely, resulting in higher water repellency. **C5⊃H** with no fluorine atoms also forms the alkyl layer structure (**Fig. S49c**), indicating that aggregation of fluorine atoms affects the increase in water repellency of **F5⊃H**.

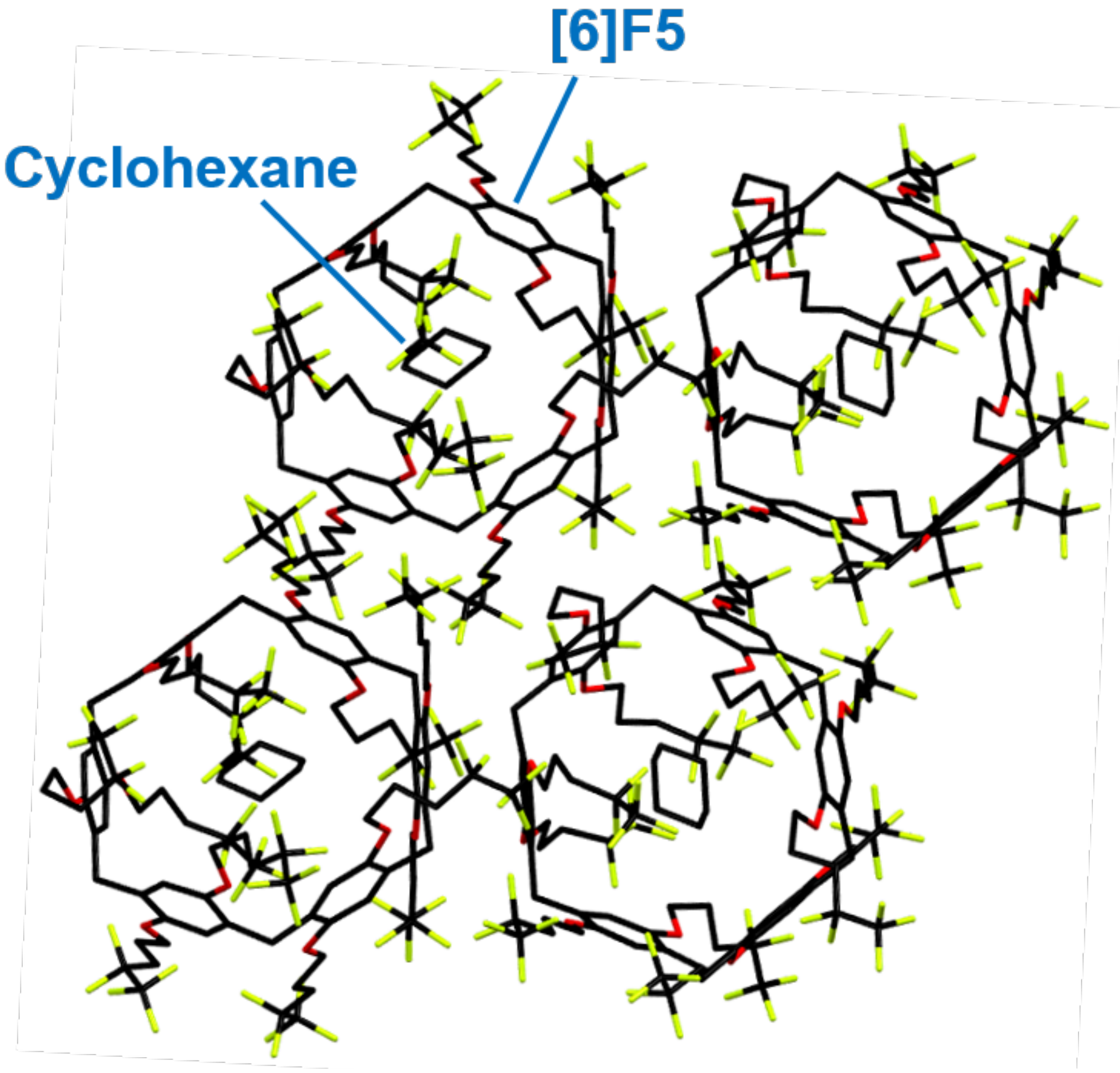


**Fig. S58** Single-crystal structure of **[6]F5⊃cyclohexane**; F, O and C atoms are represented by yellow, red and black capped sticks, respectively. Hydrogen atoms are omitted for clarity.

**[6]F5** formed 1:1 host–guest complex with cyclohexane.

**Table S8** Crystallographic data for **F5⊃H**, **F3⊃H**, **C5⊃H**, **F5⊃P**, **[6]F5⊃CyH**, and **Monomer Unit**.

| | **F5⊃H** = **F5**•$C_6H_{14}$ (CCDC-2121265) | **F3⊃H** = **F3**•$C_6H_{14}$ (CCDC-2121264) | **C5⊃H** = **C5**•$C_6H_{14}$ (CCDC-2121263) |
|---|---|---|---|
| Formula | $C_{91}H_{94}F_{50}O_{10}$ | $C_{81}H_{94}F_{30}O_{10}$ | $C_{91}H_{144}O_{10}$ |
| Formula weight | 2297.66 | 1797.56 | 1398.05 |
| Temperature (K) | 90 | 90 | 90 |
| Crystal size (mm$^3$) | 0.50 × 0.20 × 0.07 | 0.30 × 0.13 × 0.10 | 0.50 × 0.30 × 0.30 |
| Crystal system | triclinic | monoclinic | triclinic |
| Space group | $P\bar{1}$ | $P2_1/a$ | $P\bar{1}$ |
| $a$ (Å) | 20.9282(12) | 23.6441(11) | 11.9787(5) |
| $b$ (Å) | 22.7403(13) | 22.5243(11) | 17.3956(7) |
| $c$ (Å) | 24.2682(14) | 31.1470(16) | 22.0177(9) |
| $\alpha$ (deg) | 98.976(2) | 90 | 110.0599(10) |
| $\beta$ (deg) | 98.951(2) | 95.0726(19) | 90.8994(13) |
| $\gamma$ (deg) | 114.0170(17) | 90 | 101.3765(11) |
| $V$ (Å$^3$) | 10108.6(10) | 16522.9(14) | 4207.6(3) |
| $Z$ | 4 | 8 | 2 |
| $D_{calcd}$ (g cm$^{-3}$) | 1.510 | 1.445 | 1.103 |
| Collected reflections | 151621 | 298974 | 77809 |
| Unique reflections | 35639 | 29141 | 14818 |
| $R_{int}$ | 0.0681 | 0.0898 | 0.0370 |
| $2\theta_{max}$ (deg) | 134.16 | 133.38 | 134.05 |
| $F_{000}$ | 4680 | 7440 | 1540 |
| $\mu$(Cu K$\alpha$) (mm$^{-1}$) | 1.432 | 1.226 | 0.538 |
| Limiting indices | $-24 \le h \le 24$ | $-28 \le h \le 28$ | $-13 \le h \le 14$ |
| | $-27 \le k \le 27$ | $-23 \le k \le 26$ | $-20 \le k \le 20$ |
| | $-25 \le l \le 28$ | $-37 \le l \le 37$ | $-26 \le l \le 26$ |
| Restraints/parameters | 3622/3378 | 12578/3828 | 85/969 |
| Goodness of fit ($F^2$) | 1.025 | 1.129 | 1.021 |
| $R1$ ($I$>2$\sigma(I)$)[a] | 0.0784 | 0.1042 | 0.0457 |
| $wR2$ ($I$>2$\sigma(I)$)[a] | 0.2190 | 0.2322 | 0.1243 |
| $R1$ (all data)[a] | 0.0950 | 0.1406 | 0.0470 |
| $wR2$ (all data)[a] | 0.2370 | 0.2552 | 0.1257 |

[a] $R1 = \Sigma||F_o| - |F_c||/|F_o|$; $wR2 = \{\Sigma w(F_o^2 - F_c^2)^2/\Sigma[w(F_o^2)^2]\}^{1/2}$.

**Table S8** continued.

| | **F5⊃P** = **F5**•1.13$C_5H_{12}$ (CCDC-2121266) | **[6]F5⊃cyclohexane** = **[6]F5**•$C_6H_{12}$ (CCDC-2144343) | **Monomer Unit** (CCDC-2121267) |
|---|---|---|---|
| Formula | $C_{90.65}H_{93.56}F_{50}O_{10}$ | $C_{108}H_{108}F_{60}O_{12}$ | $C_{16}H_{16}F_{10}O_2$ |
| Formula weight | 2293.01 | 2737.94 | 430.29 |
| Temperature (K) | 105 | 120 | 138 |
| Crystal size (mm$^3$) | 0.64 × 0.45 × 0.10 | 0.56 × 0.52 × 0.12 | 0.40 × 0.26 × 0.07 |
| Crystal system | monoclinic | monoclinic | monoclinic |
| Space group | $P2_1/n$ | $C2/c$ | $P2_1/a$ |
| $a$ (Å) | 22.9793(16) | 69.979(2) | 11.164(3) |
| $b$ (Å) | 21.8597(16) | 13.9205(5) | 5.0419(8) |
| $c$ (Å) | 40.474(3) | 24.2019(8) | 15.9267(17) |
| $\alpha$ (deg) | 90 | 90 | 90 |
| $\beta$ (deg) | 102.220(3) | 96.4154(12) | 91.317(7) |
| $\gamma$ (deg) | 90 | 90 | 90 |
| $V$ (Å$^3$) | 19870(2) | 23428.4(14) | 896.2(3) |
| $Z$ | 8 | 8 | 2 |
| $D_{calcd}$ (g cm$^{-3}$) | 1.533 | 1.552 | 1.594 |
| Collected reflections | 222927 | 128875 | 10800 |
| Unique reflections | 34889 | 20728 | 1614 |
| $R_{int}$ | 0.0737 | 0.0564 | 0.0759 |
| $2\theta_{max}$ (deg) | 133.74 | 133.40 | 136.06 |
| $F_{000}$ | 9340 | 11136 | 436 |
| $\mu$(Cu K$\alpha$) (mm$^{-1}$) | 1.455 | 1.479 | 1.570 |
| Limiting indices | $-27 \le h \le 23$ | $-83 \le h \le 83$ | $-13 \le h \le 13$ |
| | $-25 \le k \le 26$ | $-16 \le k \le 16$ | $-5 \le k \le 6$ |
| | $-48 \le l \le 48$ | $-26 \le l \le 28$ | $-19 \le l \le 19$ |
| Restraints/parameters | 7881/3939 | 1847/2132 | 0/127 |
| Goodness of fit ($F^2$) | 1.026 | 1.015 | 1.083 |
| $R1$ ($I$>2$\sigma(I)$)[a] | 0.0996 | 0.0578 | 0.0785 |
| $wR2$ ($I$>2$\sigma(I)$)[a] | 0.2777 | 0.1649 | 0.2340 |
| $R1$ (all data)[a] | 0.1222 | 0.0657 | 0.0882 |
| $wR2$ (all data)[a] | 0.3055 | 0.1747 | 0.2479 |

[a] $R1 = \Sigma||F_o| - |F_c||/|F_o|$; $wR2 = \{\Sigma w(F_o^2 - F_c^2)^2/\Sigma[w(F_o^2)^2]\}^{1/2}$.

## 13. References


S1 Gaussian 16, Revision C.01, M. J. Frisch, G. W. Trucks, H. B. Schlegel, G. E. Scuseria, M. A. Robb, J. R. Cheeseman, G. Scalmani, V. Barone, G. A. Petersson, H. Nakatsuji, X. Li, M. Caricato, A. V. Marenich, J. Bloino, B. G. Janesko, R. Gomperts, B. Mennucci, H. P. Hratchian, J. V. Ortiz, A. F. Izmaylov, J. L. Sonnenberg, D. Williams-Young, F. Ding, F. Lipparini, F. Egidi, J. Goings, B. Peng, A. Petrone, T. Henderson, D. Ranasinghe, V. G. Zakrzewski, J. Gao, N. Rega, G. Zheng, W. Liang, M. Hada, M. Ehara, K. Toyota, R. Fukuda, J. Hasegawa, M. Ishida, T. Nakajima, Y. Honda, O. Kitao, H. Nakai, T. Vreven, K. Throssell, J. A. Montgomery, Jr., J. E. Peralta, F. Ogliaro, M. J. Bearpark, J. J. Heyd, E. N. Brothers, K. N. Kudin, V. N. Staroverov, T. A. Keith, R. Kobayashi, J. Normand, K. Raghavachari, A. P. Rendell, J. C. Burant, S. S. Iyengar, J. Tomasi, M. Cossi, J. M. Millam, M. Klene, C. Adamo, R. Cammi, J. W. Ochterski, R. L. Martin, K. Morokuma, O. Farkas, J. B. Foresman, and D. J. Fox, Gaussian, Inc., Wallingford CT, 2019.

S2 S. M. Akrami, H. Nakayachi, T. Watanabe-Nakayama, H. Asakawa, T. Fukuma, *Nanotechnology* 2014, **25**, 455701.

S3 G. M. Sheldrick, *Acta Crystallogr., Sect. C: Struct. Chem.* 2015, **71**, 3−8.

S4 N. Erdeljac, G. Kehr, M. Ahlqvist, L. Knerr, R. Gilmour, *Chem. Commun.* 2018, **54**, 12002–12005.

S5 Y. Liu, D. Tang, K. Zhang, P. Huang, Z. Wang, K. Zhu, Z. Li, L. Yuan, J. Fan, Y. Zhou, B. Song, *ACS Omega.* 2017, **2**, 2489–2498.

S6 T. Ogoshi, K. Kitajima, T. Aoki, S. Fujinami, T. Yamagishi, Y. Nakamoto, *J. Org. Chem.* 2010, **75**, 3268–3273.

S7 Y. Mi, J. Ma, W. Liang, C. Xiao, W. Wu, D. Zhou, J. Yao, W. Sun, J. Sun, G. Gao, X. Chen, J. J. Chruma, C. Yang, *J. Am. Chem. Soc.* 2021, **143**, 1553–1561.

S8 K. Jie, M. Liu, Y. Zhou, M. A. Little, A. Pulido, S. Y. Chong, A. Stephenson, A. R. Hughes, F. Sakakibara, T. Ogoshi, F. Blanc, G. M. Day, F. Huang, A. I Cooper, *J. Am. Chem. Soc.* 2018, **140**, 6921–6930.

S9 B. Li, K. Xu, Y. Wang, H. Su, L. Cui, C. Li, *RSC Adv.* 2020, **10**, 45112–45115.